

# Sparse Signal Reconstruction via ECME Hard Thresholding

Kun Qiu and Aleksandar Dogandžić, *Senior Member, IEEE*

**Abstract**—We propose a probabilistic model for sparse signal reconstruction and develop several novel algorithms for computing the maximum likelihood (ML) parameter estimates under this model. The measurements follow an underdetermined linear model where the regression-coefficient vector is the sum of an unknown deterministic sparse signal component and a zero-mean white Gaussian component with an unknown variance. Our reconstruction schemes are based on an *expectation-conditional maximization either (ECME) iteration* that aims at maximizing the likelihood function with respect to the unknown parameters for a given signal sparsity level. Compared with the existing iterative hard thresholding (IHT) method, the ECME algorithm contains an additional multiplicative term and guarantees monotonic convergence for a wide range of sensing (regression) matrices. We propose a *double overrelaxation (DORE) thresholding* scheme for accelerating the ECME iteration. We prove that, under certain mild conditions, the ECME and DORE iterations converge to local maxima of the likelihood function. The ECME and DORE iterations can be implemented exactly in small-scale applications and for the important class of large-scale sensing operators with orthonormal rows used e.g., partial fast Fourier transform (FFT). If the signal sparsity level is *unknown*, we introduce an *unconstrained sparsity selection (USS) criterion* and a *tuning-free automatic double overrelaxation (ADORE) thresholding* method that employs USS to estimate the sparsity level. We compare the proposed and existing sparse signal reconstruction methods via one-dimensional simulation and two-dimensional image reconstruction experiments using simulated and real X-ray CT data.

**Index Terms**—Expectation-conditional maximization either (ECME) algorithm, iterative hard thresholding, sparse signal reconstruction, successive overrelaxation, unconstrained sparsity selection.

## I. INTRODUCTION

**S**PARSITY is an important concept in modern signal processing. Sparse signal processing methods have been developed and applied to biomagnetic and magnetic resonance imaging [1], wireless sensing [2], spectral estimation [3], and compressive sampling (CS) [4]–[7]. For noiseless measurements, the major sparse signal reconstruction task is finding the

sparsest solution of an underdetermined linear system  $\mathbf{y} = H\mathbf{s}$  (see e.g., [8, eq. (2)]):

$$(P_0) : \quad \min_{\mathbf{s}} \|\mathbf{s}\|_0 \quad \text{subject to } \mathbf{y} = H\mathbf{s} \quad (1)$$

where  $\mathbf{y}$  is an  $N \times 1$  measurement vector,  $H$  is a known  $N \times m$  full-rank *sensing matrix* with  $N \leq m$ ,  $\mathbf{s}$  is an  $m \times 1$  unknown *signal vector*, and  $\|\mathbf{s}\|_0$  counts the number of nonzero elements in the signal vector  $\mathbf{s}$ . Exactly solving the  $(P_0)$  problem (1) requires combinatorial search and is known to be NP-hard [9].

Various tractable approaches for finding sparse solutions to underdetermined linear systems can be roughly divided into three groups: convex relaxation, greedy pursuit, and probabilistic methods. Convex methods replace the  $\ell_0$ -norm penalty with the  $\ell_1$ -norm penalty and solve the resulting convex optimization problem. Basis pursuit (BP) directly substitutes  $\ell_0$  with  $\ell_1$  in the  $(P_0)$  problem, see [10]. To combat measurement noise and accommodate for approximately sparse signals, several methods with various optimization objectives have been suggested, e.g., basis pursuit denoising (BPDN) [10], [11] and Dantzig selector [12]. The gradient projection for sparse reconstruction (GPSR), fixed-point continuation active set (FPC<sub>AS</sub>), and approximate message passing (AMP) algorithms in [13]–[15] solve the unconstrained version of the BPDN problem in a computationally efficient manner. Greedy pursuit methods approximate the  $(P_0)$  solution in an iterative manner by making locally optimal choices. Orthogonal matching pursuit (OMP) [16]–[18], compressive sampling matching pursuit (CoSAMP) [19], and iterative thresholding schemes [20]–[24] belong to this category. Probabilistic methods use full probabilistic models and statistical inference tools to solve the sparse signal reconstruction problem. Examples of the methods in this group are: Sparse Bayesian learning (SBL) [25], Bayesian compressive sensing (BCS) [26] and expansion-compression variance-component based method (ExCOV) [27].

Iterative hard thresholding (IHT) and normalized iterative hard thresholding (NIHT) algorithms in [22]–[24] (see also [21]) have attracted significant attention due to their low computation and memory requirements and theoretical and empirical evidence of good reconstruction performance. The IHT and NIHT methods require only matrix-vector multiplications and *do not* involve matrix-matrix products, matrix inversions, or solving linear systems of equations. However, they converge slowly, demanding a fairly large number of iterations, require tuning the signal sparsity level, and are sensitive to scaling of the sensing matrix (IHT) or require adaptive adjustments in each iteration to compensate for the scaling problem (NIHT).

Manuscript received January 14, 2012; accepted May 24, 2012. Date of publication June 08, 2012; date of current version August 07, 2012. The associate editor coordinating the review of this manuscript and approving it for publication was Prof. Trac D. Tran. This work was supported by the National Science Foundation under Grant CCF-0545571.

The authors are with the Department of Electrical and Computer Engineering, Iowa State University, Ames, IA 50011 USA (e-mail: kqiu@iastate.edu; qiukun.fudan@gmail.com; ald@iastate.edu).

Color versions of one or more of the figures in this paper are available online at <http://ieeexplore.ieee.org>.

Digital Object Identifier 10.1109/TSP.2012.2203818

The  $\ell_0$ -norm alternate projection method ( $\ell_0$ -AP) in [20] generalizes the IHT algorithms by replacing the transpose of the sensing matrix  $H^T$  in the IHT iteration<sup>1</sup> with the Moore-Penrose inverse of  $H$ . Indeed, if the rows of the sensing matrix  $H$  are *orthonormal*, then the  $\ell_0$ -AP iteration is equivalent to the IHT iteration in [23, eq. 10].

The contribution of this paper is four-fold.

1. Probabilistic model We propose a probabilistic framework for sparse signal reconstruction based on a random Gaussian signal model [28], [29]. We develop several novel algorithms for this model based on an *expectation-conditional maximization either (ECME) iteration* for computing the maximum likelihood (ML) parameter estimates, see also [28]. Our ECME iteration is closely related to the IHT and  $\ell_0$ -AP algorithms, see also the discussion in Section II-A. This probabilistic model enables us to employ statistical signal processing tools, such as parameter-space overrelaxation for accelerating algorithm convergence and model selection for automatically determining the signal sparsity level.

2. Convergence acceleration We develop a *double overrelaxation (DORE) thresholding* method that interleaves two successive overrelaxation steps with ECME steps, see also [29]. DORE *accelerates* the convergence of the ECME algorithm. The line searches in the overrelaxation steps have *closed-form* solutions, making these steps computationally efficient.

3. Convergence Analysis We study the convergence properties of the ECME and DORE algorithms. We prove that both algorithms converge monotonically to the local maximum of the marginal likelihood function under some fairly mild conditions. Our ECME and DORE convergence conditions are *invariant* to invertible linear transforms of the rows of  $H$  and, therefore, to scaling of  $H$  as well by a nonzero constant.

4. Signal sparsity level selection Most sparse reconstruction methods require *tuning* [30], where the tuning parameters are typically the noise or signal sparsity levels: the IHT, NIHT, and  $\ell_0$ -AP algorithms require knowledge of the signal sparsity level. In this paper, we propose an *automatic double overrelaxation (ADORE) thresholding* method that *does not* require the knowledge of the signal sparsity level. To *automatically* select the sparsity level (i.e., estimate it from the data), we introduce an *unconstrained sparsity selection (USS) criterion*. We prove that, for sparse signal and noiseless measurements, the unconstrained model selection criterion USS is *equivalent* to the constrained ( $P_0$ ) problem (1). ADORE combines the USS criterion with the DORE iteration and applies a golden-section search to maximize the USS objective function.

The rest of the paper is organized as follows. In Section II, we introduce our two-stage hierarchical probabilistic model and the ECME hard thresholding algorithm (Section II-A). In Section III, we describe the DORE thresholding method

for accelerating the convergence of the ECME iteration. In Section IV, we introduce the USS criterion and our ADORE thresholding scheme (Section IV-A) for tuning-free reconstruction. Our convergence analyses of the ECME and DORE algorithms are presented in Section V. In Section VI, we compare the performances of the proposed and existing large-scale sparse reconstruction methods using one-dimensional simulation and two dimensional image reconstruction examples from simulated and real X-ray computed tomography (CT) data. Concluding remarks are given in Section VII.

### Notation and Terminology

The multivariate probability density function (pdf) of a real-valued Gaussian random vector  $\mathbf{y}$  with mean vector  $\boldsymbol{\mu}$  and covariance matrix  $\Sigma$  is denoted by  $\mathcal{N}(\mathbf{y}; \boldsymbol{\mu}, \Sigma)$ . The absolute value,  $\ell_p$  norm, determinant, and transpose are denoted by  $|\cdot|$ ,  $\|\cdot\|_p$ ,  $\det(\cdot)$ , and  ${}^{cT}$ , respectively. The smallest integer larger than or equal to a real number  $x$  is  $\lceil x \rceil$ ;  $I_n$ ,  $\mathbf{0}_{n \times 1}$ , and  $\mathbf{0}_{n \times m}$  are the identity matrix of size  $n$ , the  $n \times 1$  vector of zeros, and the  $n \times m$  matrix of zeros, respectively;  $\lambda_{\min}(X)$  and  $\lambda_{\max}(X)$  are the minimum and maximum eigenvalues of a real-valued symmetric square matrix  $X$ ;  $\text{spark}(H)$  is the smallest number of linearly dependent columns of a matrix  $H$  [8];  $H_A$  denotes the *restriction* of the matrix  $H$  to the index set  $A$ , e.g., if  $A = \{1, 2, 5\}$ , then  $H_A = [\mathbf{h}_1 \mathbf{h}_2 \mathbf{h}_5]$ , where  $\mathbf{h}_i$  is the  $i$ th column of  $H$ ;  $\mathbf{s}_A$  is the restriction of a column vector  $\mathbf{s}$  to the index set  $A$ , e.g., if  $A = \{1, 2, 5\}$ , then  $\mathbf{s}_A = [s_1, s_2, s_5]^T$ , where  $s_i$  is the  $i$ th element of  $\mathbf{s}$ . The size of a set  $A$  is denoted by  $\dim(A)$  and  $\text{supp}(\mathbf{x})$  returns the support set of a vector  $\mathbf{x}$ , i.e., the index set corresponding to the nonzero elements of  $\mathbf{x}$ , e.g.,  $\text{supp}([0, 1, -5, 0, 3, 0]^T) = \{2, 3, 5\}$ . The thresholding operator  $\mathcal{T}_r(\mathbf{x})$  keeps the  $r$  largest-magnitude elements of a vector  $\mathbf{x}$  intact and sets the rest to zero, e.g.,  $\mathcal{T}_2([0, 1, -5, 0, 3, 0]^T) = [0, 0, -5, 0, 3, 0]^T$ .

We refer to an  $N \times m$  sensing matrix  $H$  as *proper* if it has full rank and

$$N \leq m \quad (2)$$

which implies that the rank of  $H$  is equal to  $N$ . Throughout this paper, we assume that sensing matrices  $H$  are proper, which is satisfied in almost all practical sparse signal reconstruction scenarios.

## II. PROBABILISTIC MODEL AND THE ECME ALGORITHM

We model a  $N \times 1$  real-valued measurement vector  $\mathbf{y}$  as

$$\mathbf{y} = H \mathbf{z} \quad (3a)$$

where  $H$  is an  $N \times m$  real-valued proper sensing matrix,  $\mathbf{z}$  is an  $m \times 1$  multivariate Gaussian vector with pdf

$$p_{\mathbf{z}}(\mathbf{z} | \boldsymbol{\theta}) = \mathcal{N}(\mathbf{z}; \mathbf{s}, \sigma^2 I_m) \quad (3b)$$

$\mathbf{s} = [s_1, s_2, \dots, s_m]^T$  is an *unknown*  $m \times 1$  real-valued sparse signal vector containing *at most*  $r$  nonzero elements ( $r \leq m$ ), and  $\sigma^2$  is an unknown *variance-component parameter*; we refer

<sup>1</sup>The basic IHT iteration is defined in [23, eq. (10)], where  $\Phi$  in [23] corresponds to the sensing matrix  $H$  here.

to  $r$  as the *sparsity level* of the signal and to the signal  $\mathbf{s}$  as being  $r$ -sparse. Note that  $\|\mathbf{s}\|_0 = \dim(\text{supp}(\mathbf{s}))$  counts the number of nonzero elements in  $\mathbf{s}$ ; we refer to  $\|\mathbf{s}\|_0$  as the *support size* of  $\mathbf{s}$ . Therefore, the support size  $\|\mathbf{s}\|_0$  of the  $r$ -sparse vector  $\mathbf{s}$  is less than or equal to the sparsity level  $r$ . The set of unknown parameters is

$$\boldsymbol{\theta} = (\mathbf{s}, \sigma^2) \in \Theta_r \quad (4)$$

with the parameter space  $\Theta_r = \mathcal{S}_r \times [0, +\infty)$ , where

$$\mathcal{S}_r = \{\mathbf{s} \in \mathbb{R}^m : \|\mathbf{s}\|_0 \leq r\} \quad (5)$$

is the sparse signal parameter space. The above random Gaussian signal model can be used to describe approximately sparse signals. Despite its practical importance, the random signal scenario has been neglected in the sparse signal reconstruction and compressive sampling literature, which is heavily biased towards the standard signal-plus-noise model. It is important to design reconstruction algorithms specifically for this scenario because they will outperform the standard reconstruction schemes that ignore the underlying structure of the random signal model; see our results in Section VI-A where we demonstrate such performance improvements when the rows of the sensing matrix are correlated.

The marginal likelihood function of  $\boldsymbol{\theta}$  is obtained by *integrating  $\mathbf{z}$  out* [see (3)]:

$$p_{\mathbf{y}|\boldsymbol{\theta}}(\mathbf{y}|\boldsymbol{\theta}) = \mathcal{N}(\mathbf{y}; H\mathbf{s}, \sigma^2 H H^T) \quad (6a)$$

where the fact that  $H$  is a proper sensing matrix ensures that  $H H^T$  is invertible and, consequently, that the pdf (6a) exists. For a given sparsity level  $r$ , the ML estimate of  $\boldsymbol{\theta}$  is

$$\hat{\boldsymbol{\theta}}_{\text{ML}}(r) = (\hat{\mathbf{s}}_{\text{ML}}(r), \hat{\sigma}_{\text{ML}}^2(r)) = \arg \max_{\boldsymbol{\theta} \in \Theta_r} p_{\mathbf{y}|\boldsymbol{\theta}}(\mathbf{y}|\boldsymbol{\theta}). \quad (6b)$$

For any fixed  $\mathbf{s}$ , the marginal likelihood (6a) is maximized by

$$\hat{\sigma}^2(\mathbf{s}) = \frac{(\mathbf{y} - H\mathbf{s})^T (H H^T)^{-1} (\mathbf{y} - H\mathbf{s})}{N}. \quad (7)$$

Therefore, maximizing (6a) with respect to  $\boldsymbol{\theta}$  is equivalent to first maximizing the *concentrated likelihood function*

$$p_{\mathbf{y}|\boldsymbol{\theta}}(\mathbf{y}|\mathbf{s}, \hat{\sigma}^2(\mathbf{s})) = \frac{[\hat{\sigma}^2(\mathbf{s})]^{-0.5N} \exp(-0.5N)}{\sqrt{\det(2\pi H H^T)}} \quad (8)$$

with respect to  $\mathbf{s} \in \mathcal{S}_r$ , yielding  $\hat{\mathbf{s}}_{\text{ML}}(r)$ , and then determining the ML estimate of  $\sigma^2$  by substituting  $\hat{\mathbf{s}}_{\text{ML}}(r)$  into (7). Obtaining the exact ML estimate  $\hat{\boldsymbol{\theta}}_{\text{ML}}(r)$  in (6b) requires a combinatorial search and is therefore infeasible in practice. In the following, we present a computationally feasible iterative approach that aims at maximizing (6a) with respect to  $\boldsymbol{\theta} \in \Theta_r$  and circumvents the combinatorial search.

#### A. ECME Algorithm for Known Sparsity Signal Level $r$

We treat  $\mathbf{z}$  as the *missing (unobserved) data* and present an ECME algorithm that approximately finds the ML estimate in (6b) for a fixed signal sparsity level  $r$ . Since  $r$  is assumed known, we simplify the notation and omit the dependence of the estimates of  $\boldsymbol{\theta}$  on  $r$  in this section and in Appendix A. An

ECME algorithm maximizes *either* the expected complete-data log-likelihood function (where the expectation is computed with respect to the conditional distribution of the unobserved data given the observed measurements) *or* the actual observed-data log-likelihood, see [31, Sec. 5.7].

Assume that the parameter estimate  $\boldsymbol{\theta}^{(p)} = (\mathbf{s}^{(p)}, (\sigma^2)^{(p)})$  is available, where  $p$  denotes the iteration index. *Iteration  $p + 1$*  proceeds as (see Appendix A for its derivation):

- update the sparse signal estimate using the expectation-maximization (EM) step, i.e., the expectation (E) step:

$$\begin{aligned} \mathbf{z}^{(p+1)} &= E_{\mathbf{z}|\mathbf{y}, \boldsymbol{\theta}}[\mathbf{z}|\mathbf{y}, \boldsymbol{\theta}^{(p)}] \\ &= \mathbf{s}^{(p)} + H^T (H H^T)^{-1} (\mathbf{y} - H \mathbf{s}^{(p)}) \end{aligned} \quad (9a)$$

followed by the maximization (M) step, which simplifies to

$$\mathbf{s}^{(p+1)} = \arg \min_{\mathbf{s} \in \mathcal{S}_r} \|\mathbf{z}^{(p+1)} - \mathbf{s}\|_2^2 = \mathcal{T}_r(\mathbf{z}^{(p+1)}) \quad (9b)$$

and

- update the variance component estimate using the following conditional maximization (CM) step:

$$(\sigma^2)^{(p+1)} = \frac{(\mathbf{y} - H \mathbf{s}^{(p+1)})^T (H H^T)^{-1} (\mathbf{y} - H \mathbf{s}^{(p+1)})}{N} \quad (9c)$$

obtained by maximizing the marginal likelihood (6a) with respect to  $\sigma^2$  for a fixed  $\mathbf{s} = \mathbf{s}^{(p+1)}$ , see (7).

Iterate until two consecutive sparse-signal estimates  $\mathbf{s}^{(p)}$  and  $\mathbf{s}^{(p+1)}$  do not differ significantly.

In (9a),  $E_{\mathbf{z}|\mathbf{y}, \boldsymbol{\theta}}[\mathbf{z}|\mathbf{y}, \boldsymbol{\theta}]$  denotes the mean of the pdf  $p_{\mathbf{z}|\mathbf{y}, \boldsymbol{\theta}}(\mathbf{z}|\mathbf{y}, \boldsymbol{\theta})$ , which is the Bayesian minimum mean-square error (MMSE) estimate of  $\mathbf{z}$  for *known*  $\boldsymbol{\theta}$  [32, Sec. 11.4].

The iteration (9a)–(9b) is equivalent to the  $\ell_0$ -AP scheme in [20], where it was introduced as an *ad hoc* solution to a regularized form of the  $(P_0)$  problem in (1) for a certain regularization parameter; hence, there is no underlying probabilistic model behind the method in [20]. The iteration (9a)–(9b) is also closely related to the IHT scheme in [23, eq. (10)]: The main difference is that (9a) has an additional term  $(H H^T)^{-1}$  that ensures convergence of the iteration (9a)–(9b) for a wide range of sensing matrices, see Section V. In small-scale problems with dense (e.g., random Gaussian or Bernoulli) sensing matrices  $H$ ,  $(H H^T)^{-1}$  can be pre-computed and stored, where the storage cost is  $N^2$ . Once  $(H H^T)^{-1}$  is stored, the matrix-vector product  $(H H^T)^{-1} (\mathbf{y} - H \mathbf{s}^{(p+1)})$  in each ECME iteration step costs only an additional  $\mathcal{O}(N^2)$  computations, compared to the IHT iteration whose computational complexity per iteration step is  $\mathcal{O}(N m)$ .<sup>2</sup> For large-scale problems (e.g., image and video reconstruction), it is too expensive to store  $H$  and compute  $(H H^T)^{-1}$ , thus necessitating the application of fast sampling operators. For an important class of fast sampling operators, the corresponding sensing matrices satisfy

$$H H^T = c I_N \quad (10)$$

[obviating the need to compute and store  $(H H^T)^{-1}$ ] and the large-scale ECME iteration can be implemented exactly and is equivalent to the IHT iteration in [23, eq. (12)] with step size  $\frac{1}{c}$ . For example, the partial fast Fourier transform (FFT) sampling

<sup>2</sup>Recall that we assume  $N \leq m$ , see (2).

operator satisfies (10) with  $c = 1$ , implying that the rows of the sensing matrix  $H$  are orthonormal.

1) *Approximation*: The exact ECME iteration (9) is *not feasible* in those large-scale applications where the multiplicative term  $(H H^T)^{-1}$  is general (i.e., does not have a special structure); in this case, we suggest approximating this term by a diagonal matrix or by  $\frac{1}{c}I_N$ , which corresponds to assuming that (10) holds approximately and leads to the IHT iteration in [23, eq. (12)] with step size  $\frac{1}{c}$ .

### III. THE DORE ALGORITHM FOR KNOWN SPARSITY SIGNAL LEVEL $r$

We now present our DORE algorithm that accelerates the convergence of the ECME iteration. Since the signal sparsity level  $r$  is assumed known, we omit the dependence of the estimates of  $\theta$  on  $r$  in this section.

Assume that two consecutive estimates of the unknown parameters  $\theta^{(p-1)} = (\mathbf{s}^{(p-1)}, (\sigma^2)^{(p-1)})$  and  $\theta^{(p)} = (\mathbf{s}^{(p)}, (\sigma^2)^{(p)})$  are available from the  $(p-1)$ -th and  $p$ -th iterations, respectively. *Iteration*  $p+1$  proceeds as follows:

#### 1. ECME step Compute

$$\hat{\mathbf{s}} = \mathcal{T}_r(\mathbf{s}^{(p)} + H^T (H H^T)^{-1} (\mathbf{y} - H \mathbf{s}^{(p)})) \quad (11a)$$

$$\hat{\sigma}^2 = \frac{(\mathbf{y} - H \hat{\mathbf{s}})^T (H H^T)^{-1} (\mathbf{y} - H \hat{\mathbf{s}})}{N} \quad (11b)$$

and define  $\hat{\theta} = (\hat{\mathbf{s}}, \hat{\sigma}^2)$ .

#### 2. First overrelaxation Compute the linear combination of $\hat{\mathbf{s}}$ and $\mathbf{s}^{(p)}$ :

$$\bar{\mathbf{z}} = \hat{\mathbf{s}} + \alpha_1 (\hat{\mathbf{s}} - \mathbf{s}^{(p)}) \quad (12a)$$

where the weight

$$\alpha_1 = \frac{(H \hat{\mathbf{s}} - H \mathbf{s}^{(p)})^T (H H^T)^{-1} (\mathbf{y} - H \hat{\mathbf{s}})}{(H \hat{\mathbf{s}} - H \mathbf{s}^{(p)})^T (H H^T)^{-1} (H \hat{\mathbf{s}} - H \mathbf{s}^{(p)})} \quad (12b)$$

is the *closed-form* solution of the line search:

$$\alpha_1 = \arg \max_{\alpha} p_{\mathbf{y}|\theta}(\mathbf{y} | (\hat{\mathbf{s}} + \alpha (\hat{\mathbf{s}} - \mathbf{s}^{(p)}), \sigma^2)) \quad (12c)$$

with the parameter space of  $\theta$  extended to  $\Theta_{r_1}$ , where  $r_1 = \dim(\text{supp}(\hat{\mathbf{s}}) \cup \text{supp}(\mathbf{s}^{(p)}))$  is the sparsity level of  $\hat{\mathbf{s}} + \alpha (\hat{\mathbf{s}} - \mathbf{s}^{(p)})$  and  $\sigma^2$  is an arbitrary positive number, see also (6a).

#### 3. Second overrelaxation Compute the linear combination of $\bar{\mathbf{z}}$ and $\mathbf{s}^{(p-1)}$ :

$$\tilde{\mathbf{z}} = \bar{\mathbf{z}} + \alpha_2 (\bar{\mathbf{z}} - \mathbf{s}^{(p-1)}) \quad (13a)$$

where the weight

$$\alpha_2 = \frac{(H \bar{\mathbf{z}} - H \mathbf{s}^{(p-1)})^T (H H^T)^{-1} (\mathbf{y} - H \bar{\mathbf{z}})}{(H \bar{\mathbf{z}} - H \mathbf{s}^{(p-1)})^T (H H^T)^{-1} (H \bar{\mathbf{z}} - H \mathbf{s}^{(p-1)})} \quad (13b)$$

is the closed-form solution of the line search:

$$\alpha_2 = \arg \max_{\alpha} p_{\mathbf{y}|\theta}(\mathbf{y} | (\bar{\mathbf{z}} + \alpha (\bar{\mathbf{z}} - \mathbf{s}^{(p-1)}), \sigma^2)) \quad (13c)$$

with the parameter space of  $\theta$  extended to  $\Theta_{r_2}$ , where  $r_2 = \dim(\text{supp}(\bar{\mathbf{z}}) \cup \text{supp}(\mathbf{s}^{(p-1)}))$  is the sparsity level of  $\bar{\mathbf{z}} + \alpha (\bar{\mathbf{z}} - \mathbf{s}^{(p-1)})$  and  $\sigma^2$  is an arbitrary positive number.

#### 4. Thresholding Threshold $\tilde{\mathbf{z}}$ to the sparsity level $r$ :

$$\tilde{\mathbf{s}} = \mathcal{T}_r(\tilde{\mathbf{z}}) \quad (14a)$$

compute the corresponding variance component estimate:

$$\tilde{\sigma}^2 = \frac{(\mathbf{y} - H \tilde{\mathbf{s}})^T (H H^T)^{-1} (\mathbf{y} - H \tilde{\mathbf{s}})}{N} \quad (14b)$$

and define our final overrelaxation parameter estimate  $\tilde{\theta} = (\tilde{\mathbf{s}}, \tilde{\sigma}^2)$ .

5. Decision (between ECME and thresholded overrelaxation parameter estimates) If  $p_{\mathbf{y}|\theta}(\mathbf{y} | \tilde{\theta}) \geq p_{\mathbf{y}|\theta}(\mathbf{y} | \hat{\theta})$  or, equivalently, if

$$\tilde{\sigma}^2 < \hat{\sigma}^2 \quad (15)$$

assign  $\theta^{(p+1)} = \tilde{\theta}$ ; otherwise, assign  $\theta^{(p+1)} = \hat{\theta}$  and complete *Iteration*  $p+1$ .

Iterate until two consecutive sparse-signal estimates  $\mathbf{s}^{(p)}$  and  $\mathbf{s}^{(p+1)}$  do not differ significantly. Note that the line searches in the two overrelaxation steps have *closed-form* solutions and are therefore computationally efficient. The complexity of DORE per iteration is comparable to that of ECME, but DORE converges in much fewer iterations than ECME, see the numerical examples in Section VI. The convergence guarantees we have proved in Section V for these two algorithms are the same.

Using a single successive overrelaxation step based on the most recent parameter estimate is a common approach for accelerating fixed-point iterations, however this scheme oscillates around the slowest-converging direction of the underlying EM-type iteration [33, Theorem 2], see also [33, Fig. 1], where this oscillation phenomenon is demonstrated in a two-dimensional example. Here, we adopt the idea in [33, Sec.3.3] and apply the *second overrelaxation*, which mitigates the oscillation effect and thereby converges more rapidly than the acceleration scheme based on a single successive overrelaxation. Our algorithm differs from that in [33, Sec. 3.3], which focuses on continuous parameter spaces with marginal likelihood that is differentiable with respect to the parameters. Unlike [33, Sec. 3.3], here we apply successive overrelaxation steps on parameter spaces with variable dimensions (Steps 2 and 3), threshold the second overrelaxation estimate to ensure that the resulting signal estimate is  $r$ -sparse (Step 4), and test the thresholded estimate from Step 4 versus the ECME estimate from Step 1 and adopt the better of the two (Step 5).

**DORE Initialization.** The parameter estimates  $\theta^{(1)}$  and  $\theta^{(2)}$  are obtained by applying two consecutive ECME steps (9) to an initial sparse signal estimate  $\mathbf{s}^{(0)}$ .

**The empirical Bayesian signal estimate.** We construct the following empirical Bayesian estimate of the random signal vector  $\mathbf{z}$ :

$$E_{\mathbf{z}|\mathbf{y}, \theta}[\mathbf{z} | \mathbf{y}, \theta^{(+\infty)}] = \mathbf{s}^{(+\infty)} + H^T (H H^T)^{-1} (\mathbf{y} - H \mathbf{s}^{(+\infty)}) \quad (16)$$

where  $\theta^{(+\infty)} = (\mathbf{s}^{(+\infty)}, (\sigma^2)^{(+\infty)})$  denotes the estimate of the unknown parameter set upon convergence of the DORE or ECME iterations. Unlike  $\mathbf{s}^{(+\infty)}$ , the empirical Bayesian estimate (16) is not  $r$ -sparse in general, and is therefore preferable for reconstructing nearly sparse signals that have many small

nonzero signal coefficients<sup>3</sup>; we use it for real-data X-ray CT reconstruction in Section VI-C.

Inspired by our DORE acceleration of the ECME iteration, Blumensath has recently proposed and analyzed a double overrelaxation acceleration of the IHT algorithm, see [35]. When (10) holds, this accelerated IHT scheme coincides with the above DORE iteration and can be obtained by using the approximation (10) and replacing all multiplicative terms  $(H H^T)^{-1}$  by  $\frac{1}{c}I_N$  in the DORE iteration.

#### IV. SIGNAL SPARSITY SELECTION AND THE ADORE ALGORITHM

The ECME, DORE, and most other greedy reconstruction algorithms require the knowledge of the signal sparsity level  $r$ . Here, we propose a signal sparsity selection criterion and an *automatic double overrelaxation* (ADORE) thresholding algorithm that estimates the signal sparsity level from the measurements.

We introduce the following *unconstrained sparsity selection* (USS) objective function for selecting the proper signal sparsity level  $r$  that strikes a balance between the efficiency and accuracy of signal representation:

$$\begin{aligned} \text{USS}(r) &= -\frac{1}{2} r \ln \left( \frac{N}{m} \right) \\ &\quad - \frac{1}{2} (N - r - 2) \ln_{\star} \left( \frac{\hat{\sigma}_{\text{ML}}^2(r)}{\mathbf{y}^T (H H^T)^{-1} \mathbf{y} / N} \right) \end{aligned} \quad (17)$$

where  $\hat{\sigma}_{\text{ML}}^2(r)$  is the ML estimate of the variance component  $\sigma^2$  [see (6b)],

$$\ln_{\star}(x) = \begin{cases} \ln x & x \geq \varepsilon, \\ \ln \varepsilon & x \leq \varepsilon \end{cases} \quad (18)$$

is the pseudo-logarithm function, and  $\varepsilon$  is an arbitrarily small positive constant introduced to avoid numerical problems when the ML estimate  $\hat{\sigma}_{\text{ML}}^2(r)$  is zero.<sup>4</sup> The USS objective function (17) is developed from the generalized maximum likelihood (GML) rule [36, p. 223] for model selection:

$$\text{GML}(r) = \ln p(\mathbf{y} | \hat{\boldsymbol{\theta}}_{\text{ML}}(r)) - \frac{1}{2} \ln \det [\mathcal{I}(\hat{\boldsymbol{\theta}}_{\text{ML}}(r))] \quad (19)$$

where  $\mathcal{I}(\hat{\boldsymbol{\theta}}_{\text{ML}}(r))$  is the Fisher information matrix (FIM) for the ML estimate  $\hat{\boldsymbol{\theta}}_{\text{ML}}(r)$  at the sparsity level  $r$ . The first term in (19) is a non-decreasing function of  $r$ , but the second term in (19) *penalizes* the growth of  $r$ . In Appendix B, we derive USS( $r$ ) in (17) by approximating and modifying GML so that it is computationally efficient and scale-invariant, which are desirable properties.

The USS objective (17) is closely related to the  $(P_0)$  problem (1), as shown by the following theorem.

*Theorem 1:* Suppose that we have collected a measurement vector  $\mathbf{y} = H \mathbf{s}^{\diamond}$  using a proper sensing matrix  $H$ , where  $\mathbf{s}^{\diamond}$

<sup>3</sup>In the experiment in [34, Sec. 5.2] where the approximately sparse Lena image was reconstructed from compressive samples, the empirical Bayesian estimate (16) achieved *consistently higher* (by about 1 dB) peak signal-to-noise ratios than the purely sparse signal estimate  $\mathbf{s}^{(+\infty)}$ .

<sup>4</sup>In practice,  $\varepsilon$  can be chosen as the smallest positive floating-point number of the implementation platform.

is a sparse signal vector having exactly  $r^{\diamond} = \|\mathbf{s}^{\diamond}\|_0$  nonzero elements. If

- (1) the sensing matrix  $H$  satisfies the unique representation property (URP) [3] stating that all  $N \times N$  submatrices of  $H$  are invertible or, equivalently, that

$$\text{spark}(H) = N + 1 \quad (20a)$$

and

- (2) the number of measurements  $N$  satisfies

$$N \geq \max\{2r^{\diamond}, r^{\diamond} + 3\} \quad (20b)$$

then

- USS( $r$ ) in (17) is *globally and uniquely maximized* at  $r = r^{\diamond}$  and
- the  $(P_0)$ -optimal solution and ML sparse signal estimate at  $r = r^{\diamond}$  [i.e.,  $\hat{\mathbf{s}}_{\text{ML}}(r^{\diamond})$ , see (6b)] are both *unique* and *coincide* with  $\mathbf{s}^{\diamond}$ .

*Proof:* See Appendix C.  $\square$

Theorem 1 shows that the USS objective function *transforms* the constrained optimization problem  $(P_0)$  in (1) into an equivalent unconstrained problem (17) and that, for sparse signals in the absence of noise, USS optimally selects the signal sparsity level  $r$  that allows accurate signal representation with as few nonzero signal elements as possible.

In the practical scenarios where  $r^{\diamond} \geq 3$ , (20b) reduces to  $N \geq 2r^{\diamond}$ , which is the condition required to ensure the uniqueness of the  $(P_0)$  problem, see [8, Theorem 2].

In the following, we use DORE to approximately evaluate the USS objective function and apply this approximate USS criterion to automatically select the signal sparsity level.

#### A. The ADORE Algorithm for Unknown Signal Sparsity Level $r$

We approximate the USS objective function (17) by replacing the computationally intractable ML estimate  $\hat{\sigma}_{\text{ML}}^2(r)$  with its DORE estimate. Maximizing this approximate USS objective function with respect to  $r$  by an exhaustive search may be computationally expensive because we need to apply a full DORE iteration for each sparsity level  $r$  in the set of integers between 0 and  $\frac{N}{2}$ .<sup>5</sup> Here, we propose the ADORE algorithm that applies the *golden-section search* [37, Sec. 4.5.2.1] to maximize the approximate USS objective function, with the initial search boundaries set to 0 and  $\lceil \frac{N}{2} \rceil$ . In the practical case where  $\mathbf{y} \neq \mathbf{0}_{N \times 1}$ , we have USS(0) = 0. For each candidate  $0 < r \leq \lceil \frac{N}{2} \rceil$ , we estimate  $\hat{\sigma}_{\text{ML}}^2(r)$  using the DORE iteration. After running one golden sectioning step, the length of the new search interval is approximately 0.618 of the previous interval (rounded to the closest integer). The search process ceases when the desired resolution  $L$  is reached, i.e., when the searching interval becomes shorter than the prescribed resolution level  $L$ . Therefore, ADORE requires roughly  $1.4 \lceil \log_2(\frac{N}{L}) - 1 \rceil$  full DORE iterations. For the golden-section search to find the exact maximum of a function, the function should be *unimodal*. Because we approximate USS( $r$ ) by replacing  $\hat{\sigma}_{\text{ML}}^2(r)$  with

<sup>5</sup>Note that  $\frac{N}{2}$  is the largest value of the sparsity level  $r$  for which reasonable reconstruction is possible from  $N$  measurements; otherwise, the  $(P_0)$  and ML estimates of the sparse signal may not be unique, see e.g., [8, Theorem 2].

its DORE estimate and this approximation of  $\text{USS}(r)$  is not necessarily a unimodal function of  $r$  (in general), ADORE maximizes (17) only approximately, yielding  $r_{\text{ADORE}}$ . Our ADORE sparse signal estimate is equal to the corresponding DORE estimate at  $r = r_{\text{ADORE}}$ .

## V. CONVERGENCE ANALYSIS

We now analyze the convergence properties of our ECME and DORE algorithms presented in Sections II-A and III. The analysis in this section applies only to the *exact* ECME and DORE iterations that employ the  $(H H^T)^{-1}$  multiplicative terms without approximation. The ECME algorithm in Section II-A does not satisfy the general regularity conditions assumed in standard convergence analysis of the EM-type algorithms in e.g., [31] and [38, Theorem 2]. In particular, the complete-data and conditional unobserved data given the observed data distributions  $p_{z, \mathbf{y}} | \boldsymbol{\theta}(z, \mathbf{y} | \boldsymbol{\theta})$  and  $p_{z | \mathbf{y}, \boldsymbol{\theta}}(z | \mathbf{y}, \boldsymbol{\theta})$  are both degenerate, see (3a) and Appendix A; the parameter space  $\Theta_r$  is non-convex and its interior is empty; in  $\Theta_r$ , the partial derivatives of the marginal likelihood (6a) with respect to the components of  $\mathbf{s}$  do not exist for most directions. Therefore, we establish the convergence analysis of ECME and DORE afresh here.

Maximizing the concentrated likelihood function (8) with respect to  $\mathbf{s} \in \mathcal{S}_r$  is equivalent to minimizing the weighted squared error

$$\mathcal{E}(\mathbf{s}) = N \hat{\sigma}^2(\mathbf{s}) = (\mathbf{y} - H \mathbf{s})^T (H H^T)^{-1} (\mathbf{y} - H \mathbf{s}). \quad (21)$$

The following identity holds for all  $\mathbf{s}, \mathbf{s}' \in \mathbb{R}^m$ :

$$\mathcal{E}(\mathbf{s}) = \mathcal{Q}(\mathbf{s} | \mathbf{s}') - \mathcal{H}(\mathbf{s} | \mathbf{s}') \quad (22a)$$

where

$$\mathcal{Q}(\mathbf{s} | \mathbf{s}') = \|\mathbf{s}' + H^T (H H^T)^{-1} (\mathbf{y} - H \mathbf{s}') - \mathbf{s}\|_2^2 \quad (22b)$$

$$\mathcal{H}(\mathbf{s} | \mathbf{s}') = (\mathbf{s} - \mathbf{s}')^T [I_m - H^T (H H^T)^{-1} H] (\mathbf{s} - \mathbf{s}'). \quad (22c)$$

This identity follows by rewriting (22b) as  $\mathcal{Q}(\mathbf{s} | \mathbf{s}') = \|(I_m - H^T (H H^T)^{-1} H)(\mathbf{s}' - \mathbf{s}) + H^T (H H^T)^{-1} (\mathbf{y} - H \mathbf{s}')\|_2^2$  and expanding the squares. Observe that  $\mathcal{H}(\mathbf{s} | \mathbf{s}')$  is minimized at  $\mathbf{s} = \mathbf{s}'$ . When we set  $\mathbf{s}'$  to  $\mathbf{s}^{(p)}$  (the estimate of  $\mathbf{s}$  in the  $p$ -th ECME iteration),  $\mathcal{Q}(\mathbf{s} | \mathbf{s}^{(p)}) = \|\mathbf{z}^{(p+1)} - \mathbf{s}\|_2^2$  becomes exactly the expression that is minimized in the M step (9b) and, consequently,

$$\mathcal{Q}(\mathbf{s}^{(p+1)} | \mathbf{s}^{(p)}) \leq \mathcal{Q}(\mathbf{s}^{(p)} | \mathbf{s}^{(p)}). \quad (23a)$$

Since  $\mathcal{H}(\mathbf{s} | \mathbf{s}^{(p)})$  is minimized at  $\mathbf{s} = \mathbf{s}^{(p)}$ , we have

$$\mathcal{H}(\mathbf{s}^{(p+1)} | \mathbf{s}^{(p)}) \geq \mathcal{H}(\mathbf{s}^{(p)} | \mathbf{s}^{(p)}). \quad (23b)$$

Subtracting (23a) from (23b) and using (22a) yields

$$\mathcal{E}(\mathbf{s}^{(p+1)}) \leq \mathcal{E}(\mathbf{s}^{(p)}) \quad (24)$$

and, therefore, our ECME iteration (9) ensures a *monotonically non-decreasing* marginal likelihood (6a), see also (8). Monotonic convergence is also a key general property of the EM-type algorithms [31].

Note that Step 5 of the DORE iteration (11)–(15) ensures that the resulting new parameter estimate yields the marginal likelihood function (6a) that is higher than or equal to that of the standard ECME step (Step 1). Therefore, the DORE scheme ensures monotonically nondecreasing marginal likelihood as well.

Since (21) is bounded from below by zero, the sequence  $\mathcal{E}(\mathbf{s}^{(p)})$  must converge to a limit as the iteration index  $p$  grows to infinity. However, the fact that  $\mathcal{E}(\mathbf{s}^{(p)})$  converges does not necessarily imply the convergence of  $\mathbf{s}^{(p)}$ . If  $\mathbf{s}^{(p)}$  converges, where does it converge? Is it a local or the global maximum of the marginal log-likelihood function (6a)? To answer these questions, we first define the local maximum of a function over the parameter space  $\mathcal{S}_r$  in (5).

*Definition 1 ( $r$ -Local Maximum and Minimum):* For a function  $f(\mathbf{s}) : \mathbb{R}^m \rightarrow \mathbb{R}$ , a vector  $\mathbf{s}^* \in \mathcal{S}_r$  is an  $r$ -local maximum point of  $f(\mathbf{s})$  if there exists a  $\delta > 0$ , such that, for all  $\mathbf{s} \in \mathcal{S}_r$  satisfying  $\|\mathbf{s} - \mathbf{s}^*\|_2 < \delta$ , we have

$$f(\mathbf{s}^*) \geq f(\mathbf{s}). \quad (25)$$

Then,  $f(\mathbf{s}^*)$  is the corresponding  $r$ -local maximum of  $f(\mathbf{s})$ . We define  $\mathbf{s}^* \in \mathcal{S}_r$  and  $f(\mathbf{s}^*)$  as an  $r$ -local minimum point and the corresponding  $r$ -local minimum of  $f(\mathbf{s})$  if  $\mathbf{s}^*$  is an  $r$ -local maximum point for the function  $-f(\mathbf{s})$ .

Definition 1 states that an  $r$ -sparse vector is an  $r$ -local maximum (or minimum) point of a function  $f(\mathbf{s})$  if, in some small neighborhood, this vector attains the largest (or smallest) function value among all the sparse vectors within that small neighborhood.

The following theorem establishes that, under mild conditions, ECME and DORE iterations converge to an  $r$ -local maximum point of the concentrated marginal likelihood.

*Theorem 2:* Assume that the sparsity level  $r$  satisfies

$$r \leq \frac{1}{2}(m - N) \quad (26)$$

and that the sensing matrix  $H$  satisfies the URP condition (20a). Then, the signal iterate of the ECME algorithm for sparsity level  $r$  converges monotonically to an  $r$ -local maximum point of the concentrated marginal likelihood function (8). Similarly, the signal iterate of the DORE algorithm for sparsity level  $r$  converges monotonically to an  $r$ -local maximum point of (8).

*Proof:* See Appendix D.  $\square$

Note that (26) is a mild condition. In practice,  $N \ll m$  and (26) specifies a large range of sparsity levels  $r$  for which the ECME and DORE iterations converge. Theorem 2 claims that, if  $H$  satisfies the URP condition (20a) and for a sufficiently small sparsity level  $r$ , both ECME and DORE algorithms in Sections II-A and III converge to an  $r$ -local maximum of the concentrated marginal likelihood function (8).

The conditions of Theorem 2 holds even when the sensing matrix  $H$  is pre-multiplied by a full-rank square matrix. In contrast, the convergence result of the  $\ell_0$ -AP method in [20] is restricted to the case where the Moore-Penrose inverse of  $H$  is a tight frame (see [20, Sec. 3]) and, consequently, (10) holds. The IHT algorithm converges to a local minimum of the squared residual error for a specified signal sparsity level *only* if  $H$  is appropriately scaled. Indeed, [22, Theorem 4] demands that the spectral norm of the sensing matrix  $H$  is less than unity; if this

spectral norm condition does not hold, then the IHT iteration may become unstable and diverge, see [24, Sec. II-D]. To overcome such scaling requirements and ensure convergence for an arbitrarily scaled  $H$ , a normalized IHT (NIHT) method has been proposed in [24], where an adaptive step size is introduced to the original hard thresholding step. This term is monitored and adjusted in each iteration so that it does not exceed a certain threshold. However, this monitoring and adjustment consume CPU time and typically *slow down* the resulting algorithm, see the numerical examples in Section VI. In contrast, our ECME and DORE iterations guarantee monotonic convergence for a wide range of sensing matrix  $H$  without the need for step size monitoring and adjustment.

## VI. NUMERICAL EXAMPLES

We now evaluate our proposed methods in Sections III and IV using one-dimensional simulated examples and two-dimensional X-ray computed tomographic (CT) image reconstruction experiments.

We compare the following methods:

- the DORE and ADORE<sup>6</sup> schemes initialized by the zero sparse signal estimate:

$$\mathbf{s}^{(0)} = \mathbf{0}_{m \times 1} \quad (27)$$

with MATLAB implementations available at <http://home.eng.iastate.edu/~ald/DORE.htm>;

- the ECME method in Section II-A initialized by the zero sparse signal estimate  $\mathbf{s}^{(0)}$  in (27);
- the NIHT scheme in [24], initialized by the zero sparse signal estimate  $\mathbf{s}^{(0)}$  in (27);
- the fixed-point continuation active set algorithm in [14] with the regularization parameter

$$\tau = 10^a \|\mathbf{H}^T \mathbf{y}\|_\infty \quad (28)$$

(labeled  $\text{FPC}_{\text{AS},a}$ ) that aims at minimizing the Lagrangian cost function

$$0.5 \|\mathbf{y} - \mathbf{H} \mathbf{s}\|_2^2 + \tau \|\mathbf{s}\|_1 \quad (29)$$

where  $a$  is manually tuned for good performance in each of the following two numerical examples;

- the Barzilai-Borwein version of the gradient-projection for sparse reconstruction method with debiasing in [13] with the convergence threshold  $\tau_{\text{opt}} = 10^{-5}$  and regularization parameter chosen as in (28) (labeled  $\text{GPSR}_a$ ) with  $a$  manually tuned for good performance.

Both  $\text{GPSR}$  and  $\text{FPC}_{\text{AS}}$  methods aim at solving efficiently the unconstrained version of the BPDN problem, but the latter is numerically more stable than the former in our experiments. The form of the regularization parameter  $\tau$  in (28) was suggested in [13, eq. (22)].

### A. One-Dimensional Sparse Signal Reconstruction

We have generated sparse signals  $\mathbf{s}$  of length  $m = 500$  containing  $\|\mathbf{s}\|_0 \in [10, 100]$  randomly located nonzero elements. The nonzero components of  $\mathbf{s}$  are independent, identically

<sup>6</sup>In the one-dimensional simulation (Section VI-A), the ADORE search resolution level is set to  $L = 4$ , while in the two-dimensional CT image reconstructions (Sections VI-B and VI-C),  $L$  is set to 500.

distributed (i.i.d.) samples from *Gaussian* distribution with zero mean and unit variance. The  $N \times 1$  measurement vector  $\mathbf{y}$  is generated using linear model (3), where  $N = 250$ . We consider the deterministic and random signal scenarios with  $\sigma^2 = 0$  and  $\sigma^2 = 10^{-4}$ , respectively. The  $N \times m$  sensing matrices  $H$  are simulated using a *white Gaussian sensing matrix* whose entries are i.i.d. zero-mean Gaussian random variables with variance  $\frac{1}{m}$  or a *correlated Gaussian sensing matrix* whose columns are i.i.d. zero-mean Gaussian random vectors of size  $N \times 1$  with covariance matrix  $\Gamma$  whose  $(i, j)$ th element is  $\Gamma_{i,j} = \frac{0.9^{|i-j|}}{m}$ ,  $i, j = 1, 2, \dots, N$ . The white Gaussian sensing matrix has approximately orthonormal rows and satisfies  $E_H[\mathbf{H} \mathbf{H}^T] = I_N$ . In contrast, for correlated Gaussian sensing matrices,  $E_H[\mathbf{H} \mathbf{H}^T] = m \Gamma$ . Here, we also consider two approximate DORE implementations:

- $\text{DORE}_{\text{app},1}$ , which approximates the  $(\mathbf{H} \mathbf{H}^T)^{-1}$  term by  $I_N$ , and
- $\text{DORE}_{\text{app},2}$ , which approximates the  $(\mathbf{H} \mathbf{H}^T)^{-1}$  term by  $(E_H[\mathbf{H} \mathbf{H}^T])^{-1}$ .

For white Gaussian sensing matrices,  $\text{DORE}_{\text{app},1}$  and  $\text{DORE}_{\text{app},2}$  coincide and are labeled  $\text{DORE}_{\text{app}}$ . For correlated Gaussian sensing matrices,

$$(E_H[\mathbf{H} \mathbf{H}^T])^{-1} = (m \Gamma)^{-1} = \frac{1}{(1 - 0.9^2)} \begin{bmatrix} 1 & -0.9 & & & 0 \\ -0.9 & 1 + 0.9^2 & -0.9 & & \\ & -0.9 & 1 + 0.9^2 & \ddots & \\ & & \ddots & \ddots & -0.9 \\ 0 & & & -0.9 & 1 \end{bmatrix} \quad (30)$$

which is a sparse banded matrix.<sup>7</sup>

For the ECME, DORE, ADORE, and NIHT iterations, we use the following convergence criterion:<sup>8</sup>

$$\frac{\|\mathbf{s}^{(p+1)} - \mathbf{s}^{(p)}\|_2^2}{m} < 10^{-14}. \quad (31)$$

Our performance metric is the *average* mean-square error (MSE) of a signal estimate  $\hat{\mathbf{s}}$ :

$$\text{MSE}\{\hat{\mathbf{s}}\} = \frac{E_{H, \mathbf{s}, \mathbf{y}}[\|\hat{\mathbf{s}} - \mathbf{s}\|_2^2]}{m} \quad (32)$$

computed using 500 Monte Carlo trials, where *averaging* is performed over the random sensing matrices  $H$ , the sparse signal  $\mathbf{s}$  and the measurements  $\mathbf{y}$ .

The ECME, NIHT, DORE,  $\text{DORE}_{\text{app},1}$ , and  $\text{DORE}_{\text{app},2}$  methods require knowledge of the signal sparsity level  $r$ ; here, we use  $r = \|\mathbf{s}\|_0$  to implement these algorithms. In contrast, the ADORE method is *automatic* and *estimates* the sparsity level  $r$  from the measurements using the USS criterion. We tuned the regularization parameter  $\tau$  in (28) for the  $\text{FPC}_{\text{AS},a}$  and  $\text{GPSR}_a$  methods by varying  $a$  within the set  $\{-1, -2, -3, -4, -5, -6, -7, -8, -9\}$  and, for each  $\|\mathbf{s}\|_0$  and each of the two methods, we use the optimal  $a$  that achieves the smallest average MSE; the resulting methods are labeled  $\text{FPC}_{\text{AS},\text{opt}}$  and  $\text{GPSR}_{\text{opt}}$ , respectively.

<sup>7</sup>Multiplication by the sparse banded matrix in (30) can be implemented efficiently.

<sup>8</sup>To implement the NIHT scheme, we incorporated the convergence criterion (31) into the corresponding MATLAB codes from the sparsify toolbox at <http://users.fmrib.ox.ac.uk/~tblumens/sparsify/sparsify.html>.

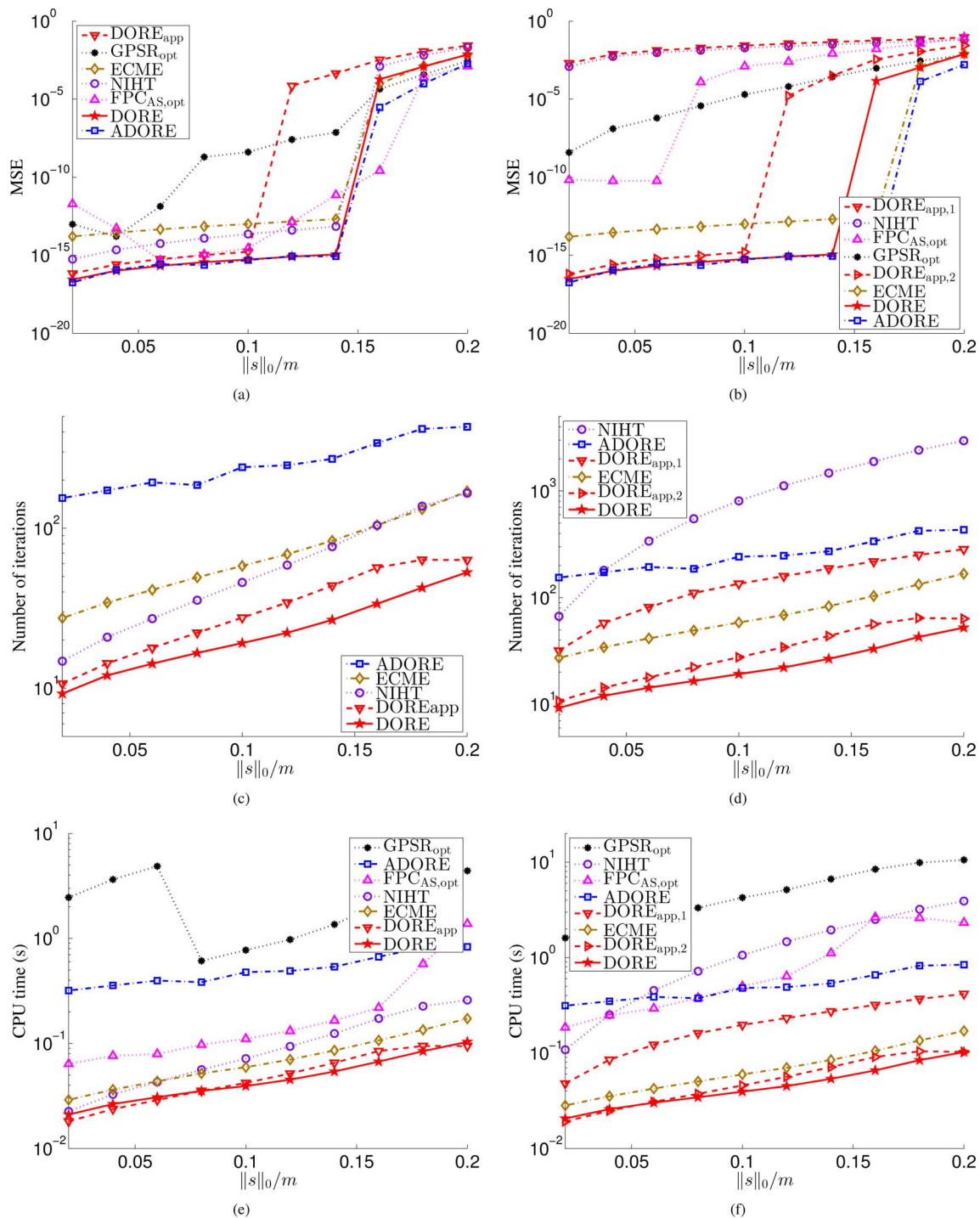


Fig. 1. (a)–(b) MSEs, (c)–(d) numbers of iterations, and (e)–(f) CPU times as functions of the sparsity ratio  $\frac{\|s\|_0}{m}$  using white [(a), (c), (e)] and correlated [(b), (d), (f)] Gaussian sensing matrices, respectively, for deterministic signal ( $\sigma^2 = 0$ ).

Fig. 1 shows the MSEs, numbers of iterations, and CPU times of various methods as functions of the sparsity ratio  $\frac{\|s\|_0}{m}$  for deterministic signal ( $\sigma^2 = 0$ ). For a large part of MSE curves, the MSEs of several methods are lower than  $10^{-10}$ , which indicates (nearly) perfect recovery. For white Gaussian sensing matrices, the MSE performances of ECME, DORE, ADORE and NIHT are similar, and the approximate  $\text{DORE}_{\text{app}}$  method achieves inferior MSEs when  $\frac{\|s\|_0}{m} = 0.12$  and  $0.14$ . Among the hard thresholding methods (ECME, DORE,  $\text{DORE}_{\text{app}}$ , ADORE and NIHT), DORE converges in the smallest number

of iterations, see Fig. 1(c). In terms of the average CPU time<sup>9</sup>, DORE and  $\text{DORE}_{\text{app}}$  are the fastest methods among all the methods compared; the ECME and NIHT methods require slightly longer time to converge and are faster than the convex methods  $\text{FPC}_{\text{AS,opt}}$  and  $\text{GPSR}_{\text{opt}}$ , see Fig. 1(c) and (e).

<sup>9</sup>For ECME, DORE, and ADORE, the matrix inverse term  $(H H^T)^{-1}$  is precomputed and the CPU time of this computation (which is around 0.027 seconds) is not counted to the CPU time of these algorithms. In practice, as long as  $H$  does not change, we need to compute  $(H H^T)^{-1}$  only once and apply it to run many ECME, DORE, and ADORE iterations.

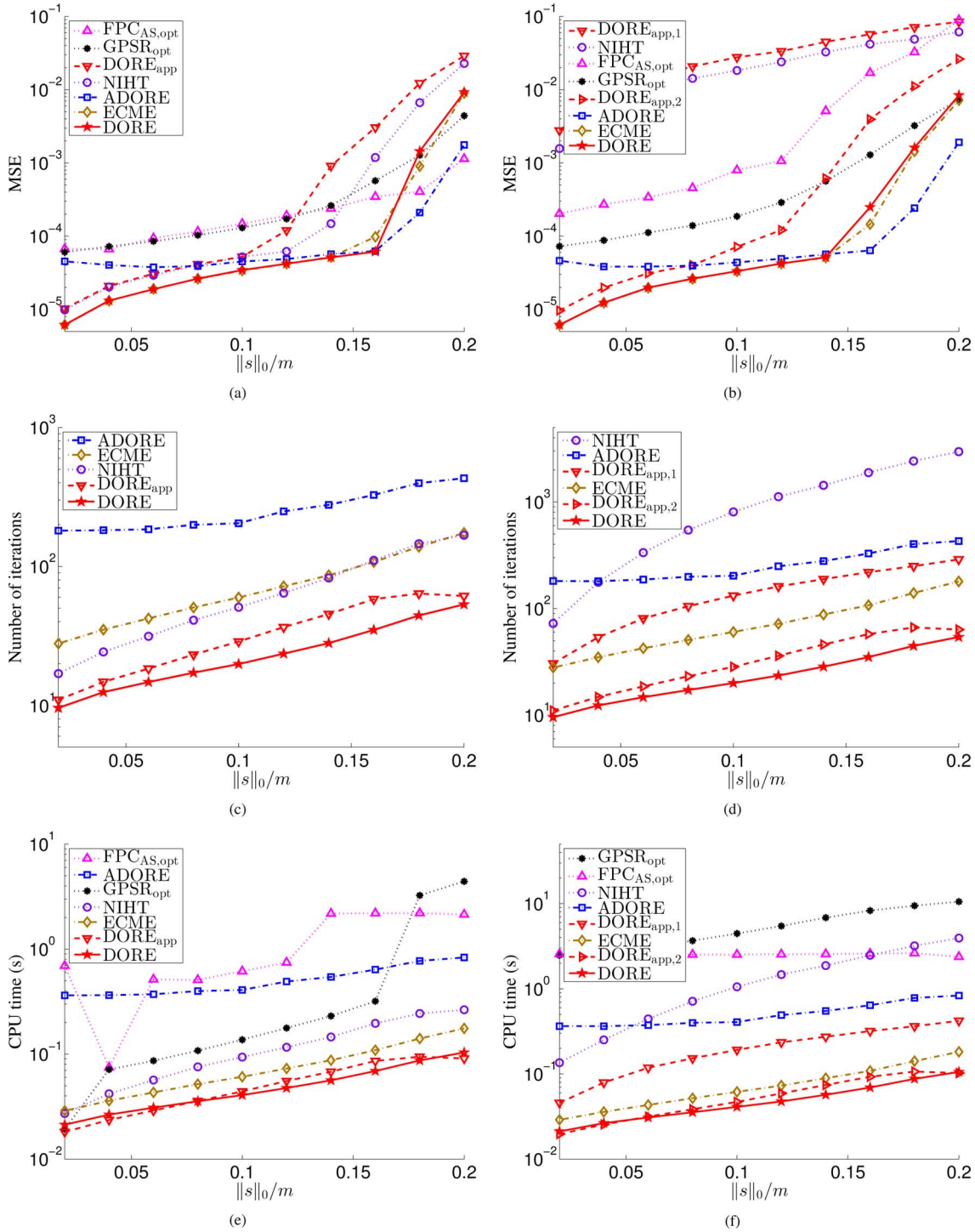


Fig. 2. (a)–(b) MSEs, (c)–(d) numbers of iterations, and (e)–(f) CPU times as functions of the sparsity ratio  $\frac{\|s\|_0}{m}$  using white [(a), (c), (e)] and correlated [(b), (d), (f)] Gaussian sensing matrices, respectively, for random signal with variance  $\sigma^2 = 10^{-4}$ .

For correlated Gaussian sensing matrices, the ECME, DORE and ADORE methods achieve significantly lower MSEs than NIHT, DORE<sub>app,1</sub>, FPC<sub>AS,opt</sub>, and GPSR<sub>opt</sub>, which do not use the multiplicative term  $(HH^T)^{-1}$ . The DORE<sub>app,2</sub> method, which uses a fairly accurate approximation of  $(HH^T)^{-1}$ , achieves quite good reconstruction accuracy, outperforming or matching all other methods except the ECME, DORE, and ADORE algorithms that employ  $(HH^T)^{-1}$ . Note that DORE and DORE<sub>app,2</sub> converge in the smallest numbers of iterations and consume the shortest

CPU runtime; in contrast, DORE<sub>app,1</sub> and NIHT require significantly more iterations and CPU time to converge, see Fig. 1(d) and (f).

Fig. 2 shows the reconstruction results for random signal with variance  $\sigma^2 = 10^{-4}$ . For the white Gaussian sensing matrix, the ECME and DORE that implement  $(HH^T)^{-1}$  exactly achieve slightly smaller MSEs than NIHT and DORE<sub>app,1</sub> that do not use this matrix inverse term, see Fig. 2(a). Interestingly, for  $\frac{\|s\|_0}{m} = 0.18$  and 0.2, the ADORE method achieves the smallest MSE among all the hard thresholding schemes. According to

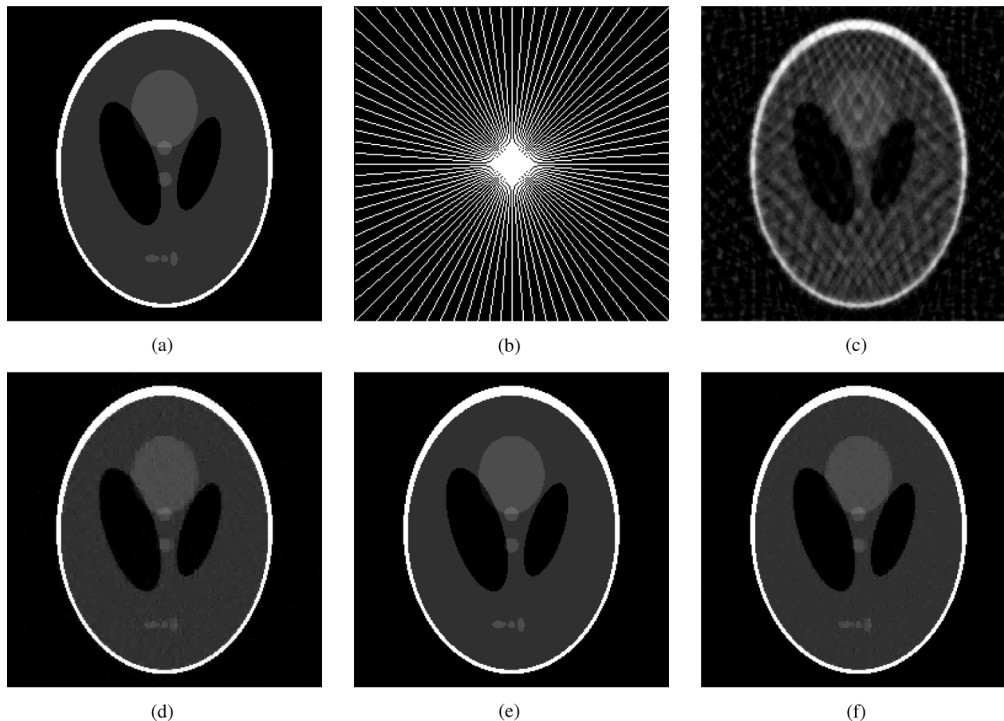


Fig. 3. (a) The size- $256^2$  Shepp-Logan phantom and the reconstruction achieved by all hard thresholding schemes, (b) a star-shaped sampling domain in the frequency plane containing 44 radial lines, and (c) the FBP, (d)  $\text{GPCR}_{-4}$ , (e)  $\text{FPC}_{\text{AS},-5}$ , and (f)  $\text{FPC}_{\text{AS},-7}$  reconstructions.

Fig. 2(c) and (e), DORE converges in smallest number of iterations among the hard thresholding methods and DORE and  $\text{DORE}_{\text{app},1}$  are the fastest in terms of CPU time among all the compared methods.

For correlated Gaussian sensing matrices, we observe again that the ECME, DORE and ADORE methods achieve significantly smaller MSEs than NIHT and  $\text{DORE}_{\text{app},1}$  that do not use the multiplicative term  $(H H^T)^{-1}$ .  $\text{DORE}_{\text{app},2}$  achieves more accurate reconstruction than  $\text{DORE}_{\text{app},1}$ , NIHT, and  $\text{FPC}_{\text{AS},\text{opt}}$ . DORE and  $\text{DORE}_{\text{app},2}$  still require the smallest number of iterations and shortest CPU runtime. Here, NIHT and  $\text{DORE}_{\text{app},1}$  need much more iterations to converge and consume much longer CPU times than for white Gaussian sensing matrices.

Under both the noiseless and noisy scenarios, the MSEs of the tuning-free ADORE method are almost as good as the ECME, DORE, and NIHT methods that have the knowledge of the true signal sparsity  $\|\mathbf{s}\|_0$ . Under the noisy scenario, DORE and ECME exhibit similar reconstruction accuracies, which is expected; under the noiseless scenario, their performances differ, but mostly in cases where both methods achieve very small average MSEs. DORE is also consistently faster than ECME; the acceleration achieved by DORE is more significant in the large-scale examples, see Sections VI-B and VI-C.

In the following, we consider simulated and real-data X-ray CT recovery experiments, respectively.

### B. Shepp-Logan Phantom Reconstruction From Simulated CT Data

The sensing matrix  $H$  has the following structure (see, e.g., [6, eq. (2) and Fig. 1]):  $H = \Phi \Psi$ , where  $\Phi$  is an  $N \times m$  sampling matrix and  $\Psi$  is an appropriate  $m \times m$  orthogonal sparsifying

transform matrix. We choose  $\Psi$  as an inverse discrete wavelet transform (DWT) matrix [39]. In this section, we also show the performance of the traditional filtered backprojection (FBP) estimate for CT reconstruction, computed as  $\hat{\mathbf{s}}_{\text{FBP}} = H^T \mathbf{y}$  [4].

For the ECME, DORE, ADORE, and NIHT iterations, we use the convergence criterion in (31).

Consider the reconstruction of the Shepp-Logan phantom of size  $m = 256^2$  in Fig. 3(a). We simulated the tomographic measurements  $\mathbf{y}$  using 2-D discrete Fourier transform (DFT) coefficients of the phantom sampled over a star-shaped domain, as illustrated in Fig. 3(b), see also [4], [24], [28], and [40]. Therefore, the sampling matrix  $\Phi$  is a *partial Fourier matrix* constructed using selected rows of the DFT matrix that yield the corresponding DFT coefficients of the phantom image within the star-shaped domain. In this example, we select  $\Psi$  as the inverse Haar (Daubechies-2) DWT matrix. The Haar wavelet transform coefficients of the phantom image in Fig. 3(a) are sparse, with  $\|\mathbf{s}\|_0 = 3769 \approx 0.06 m$ , where the true signal vector  $\mathbf{s}$  consists of the Haar wavelet transform coefficients of the phantom in Fig. 3(a). For our choices of  $\Phi$  and  $\Psi$ , the rows of  $H$  are orthonormal, i.e., (10) holds *exactly* with  $c = 1$ , implying that the ECME iteration in Section II-A is equivalent to the IHT iteration with unit step size.

We use the peak signal-to-noise ratio (PSNR) of a reconstructed image  $\Psi \hat{\mathbf{s}}$  as performance metric, where  $\hat{\mathbf{s}}$  is the estimated wavelet coefficients vector:

$$\begin{aligned} \text{PSNR (dB)} &= 10 \log_{10} \left\{ \frac{[(\Psi \mathbf{s})_{\text{MAX}} - (\Psi \mathbf{s})_{\text{MIN}}]^2}{\|\Psi \hat{\mathbf{s}} - \Psi \mathbf{s}\|_2^2} \right\} \\ &= 10 \log_{10} \left\{ \frac{[(\Psi \mathbf{s})_{\text{MAX}} - (\Psi \mathbf{s})_{\text{MIN}}]^2}{\|\hat{\mathbf{s}} - \mathbf{s}\|_2^2} \right\} \quad (33) \end{aligned}$$

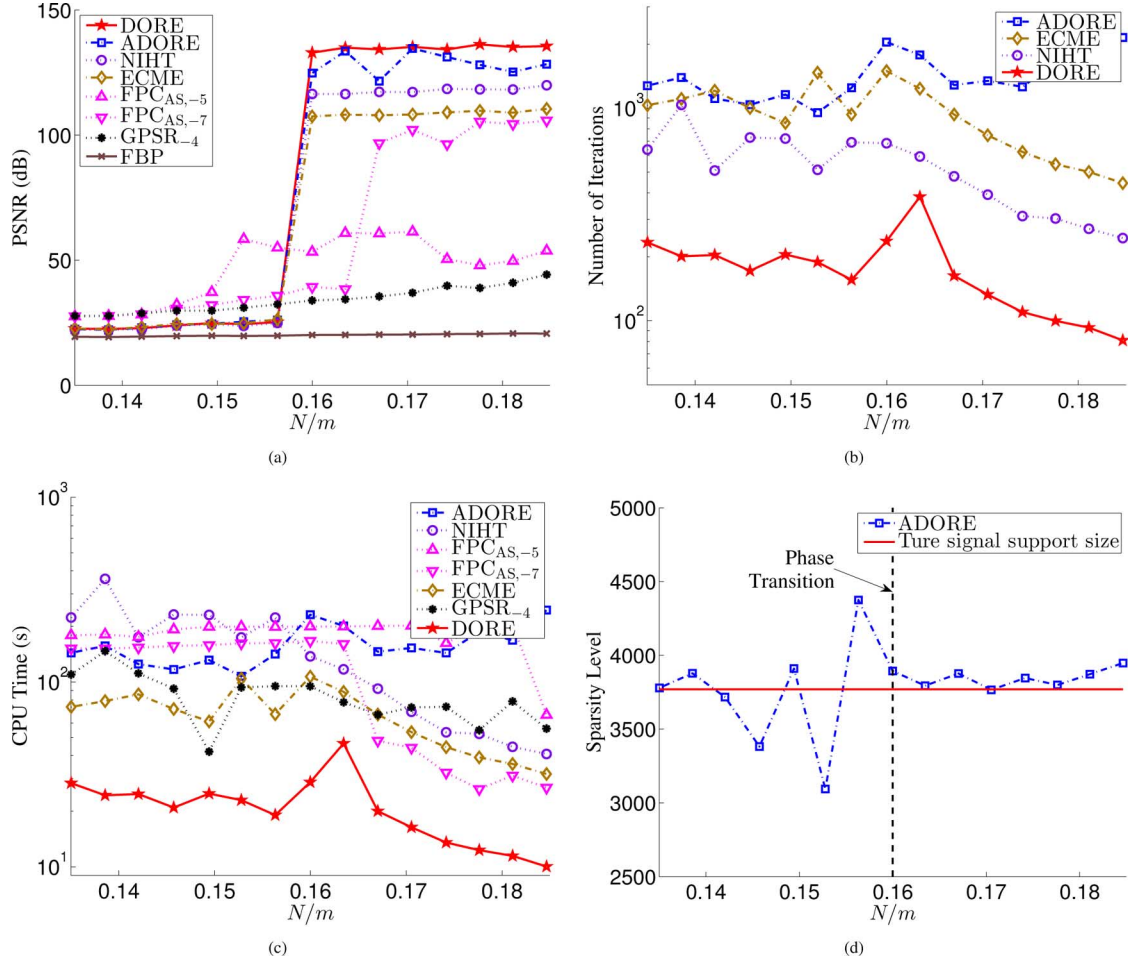


Fig. 4. (a) PSNR, (b) number of iterations, (c) CPU time, and (d) estimated signal sparsity level as functions of the normalized number of measurements  $\frac{N}{m}$  for phantom image reconstruction.

where  $(\Psi \mathbf{s})_{\min}$  and  $(\Psi \mathbf{s})_{\max}$  denote the smallest and largest elements of  $\Psi \mathbf{s}$ .

ECME, DORE, and NIHT require knowledge of the signal sparsity level  $r$ ; in this example, we set  $r$  to the true signal support size:

$$r = 3769. \quad (34)$$

In contrast, the ADORE method is *automatic* and *estimate*  $r$  from the measurements using the USS criterion.

We tuned the regularization parameter  $\tau$  in (28) for the  $\text{FPC}_{\text{AS},a}$  and  $\text{GPSR}_a$  methods by selecting  $a$  from the set

$$\{-1, -2, -3, -4, -5, -6, -7\}. \quad (35)$$

We varied  $\frac{N}{m}$  by changing the number of radial lines in the star-shaped partial Fourier sampling pattern and found that GPSR achieves the best overall PSNR for  $a = -4$  and that GPSR becomes numerically unstable for  $a \in \{-5, -6, -7\}$ .<sup>10</sup> For  $\text{FPC}_{\text{AS}}$ , the optimal value of  $a$  changes as  $\frac{N}{m}$  varies, with the best values falling in the set  $\{-5, -6, -7\}$ .  $\text{FPC}_{\text{AS},-4}$  achieves

<sup>10</sup>Even though the  $\text{GPSR}_a$  and  $\text{FPC}_{\text{AS},a}$  methods aim at solving the same convex optimization problem, in this example, their corresponding reconstructions differ greatly for  $a \in \{-5, -6, -7\}$ : the  $\text{FPC}_{\text{AS},a}$  solution achieves a much lower Lagrangian cost function (29) as well as better reconstruction accuracy than GPSR.

the same reconstruction performance as  $\text{GPSR}_{-4}$ , which is inferior to  $\text{FPC}_{\text{AS},a}$  for  $a \in \{-5, -6, -7\}$ . Fig. 3 shows the performances of  $\text{FPC}_{\text{AS},-5}$  and  $\text{FPC}_{\text{AS},-7}$ .

Parts (a) and (c)–(f) of Fig. 3 show the images reconstructed by the above methods using the 44 radial-line sampling pattern in Fig. 3(b), which corresponds to the normalized number of measurements (subsampling factor)  $\frac{N}{m} = 0.163$ . Here, all hard thresholding methods (ECME, DORE, NIHT, and ADORE) achieve perfect reconstructions of the original phantom image with PSNRs over 100 dB.  $\text{FPC}_{\text{AS},-5}$  achieves good recovery with PSNR around 60 dB. In contrast, the other methods achieve inferior reconstructions with PSNRs 20.2 dB, 34.4 dB, and 38.4 dB for the FBP,  $\text{GPSR}_{-4}$ , and  $\text{FPC}_{\text{AS},-7}$  estimates, respectively.

In Fig. 4, we vary  $\frac{N}{m}$  and show the PSNRs, numbers of iterations, and CPU times of the above methods, as well as the signal sparsity level estimate obtained by ADORE. In this example, all hard thresholding methods exhibit a sharp phase transition at  $\frac{N}{m} \approx 0.16$ .  $\text{FPC}_{\text{AS},-7}$  achieves a fairly sharp and large phase transition at  $\frac{N}{m} \approx 0.167$  whereas  $\text{FPC}_{\text{AS},-5}$  achieves an earlier but smaller phase transition at  $\frac{N}{m} \approx 0.153$ . The  $\text{GPSR}_{-4}$  method exhibits no obvious phase transition. The performance difference of  $\text{FPC}_{\text{AS},a}$  for different  $a$  shows the sensitivity of the convex methods to tuning.

ADORE performs as well as the ECME, DORE, and NIHT methods that require prior knowledge of the signal sparsity level. Indeed, Fig. 4(d) shows that the USS criterion accurately selects the signal sparsity level, particularly after the phase transition has occurred ( $\frac{N}{m} > 0.16$ ). This is consistent with the essence of Theorem 1.

Among all hard thresholding methods, DORE needs the smallest number of iterations to converge and is also the fastest in terms of the CPU time. DORE needs 3.2 to 7.8 times less iterations than ECME and 1.5 to 5.2 times less iterations than NIHT; in terms of the CPU time, DORE is 1.9 to 4.6 times faster than ECME and 2.5 to 14.8 times faster than NIHT. In addition, DORE is noticeably faster than the convex methods  $\text{FPC}_{\text{AS}}$  and GPSR.

Since only a single choice (27) is used to initialize ECME, DORE and ADORE, their PSNR curves in Fig. 4(a) are only lower bounds on the PSNRs achievable by these methods.

### C. Real-Data X-Ray CT Reconstruction

In this example, we apply our proposed methods to reconstruct an industrial object from real cone-beam X-ray CT projections. First, we performed the standard fan-to-parallel beam conversion (see [41, Sec. 3.4]) and generated parallel-beam projections with  $1^\circ$  spacing and measurement array size of 1023 elements, yielding  $N = 1024$  frequency-domain measurements per projection (upon taking FFT of each projection). To the best of our knowledge, this is one of the first applications of compressive sampling to real CT data using the standard compressive sampling model that employs the sensing matrix in the form of the product between the sampling and sparsifying transform matrices. Almost all existing CT examples of compressive sampling in e.g., [4], [24], [28], [40] and the previous example use synthetic data, such as the Shepp-Logan phantom, and approximate the CT sampling operation by selected 2-D discrete Fourier transform (DFT) coefficients of the underlying image on the uniform Cartesian grid in the 2-D spatial frequency plane. However, this approximation is crude. According to the Fourier slice theorem [41, Sec. 3.2], upon applying 1D-DFT to each of the X-ray CT projections, we obtain *discrete-space Fourier transform (DSFT)* coefficients of the underlying image along straight radial lines in the 2-D spatial frequency plane, which are *concentrated* in the center (low-frequency) region of this plane, see Figs. 5(a) and 6(a). Therefore, the approximation of the CT sampling operation in [4], [24], [28], [40] cannot be used in real X-ray CT applications, see also [40, footnote 4]. Here, we employ the non-uniform frequency-domain sampling pattern that accurately maps the X-ray CT measurements to the corresponding spatial frequency locations. Given the raw CT projection data, we first compute the FFTs of the CT projections and, after separating the real and imaginary parts, stack the real-valued FFT coefficients of all projections into the measurement vector  $\mathbf{y}$ . The corresponding sampling matrix  $\Phi$  is implemented using the *nonuniform fast Fourier transform (NUFFT)* [42], which efficiently computes the DSFT coefficients at the desired frequency locations. The orthonormal sparsifying matrix  $\Psi$  is constructed using the inverse Daubechies-6 DWT matrix and the sensing matrix  $H$  is constructed using [43]

with the full circular mask, yielding  $m = 840493$  signal elements. In this example,  $N$  is equal to 1024 times the number of CT projections, which is 180 or 160 for the two sampling scenarios in Figs. 5(a) and 6(a). Because of the nonuniform spacing of the frequency locations and the numerical interpolation employed by the NUFFT algorithm in [42], here the rows of  $H$  are only approximately orthonormal; we implement the DORE iteration using (10) with  $c$  estimated by averaging the diagonal elements of  $H H^T$ . The sampling pattern in Fig. 5(a) corresponds to the standard 180 uniform-angle X-ray CT projections and Fig. 6(a) corresponds to a *limited-angle projection scenario* where 20 out of the 180 uniform-angle projections are missing with the missing projections contiguous in two regions. The limited-angle projection scenario is motivated by the fact that, in some applications, the physical constraint of the CT scanner or the object being scanned prevents projections from certain directions [41, Sec. 6.7.6]. We have implemented the FBP method using the Hann window in the frequency domain [41, Sec. 3.3]. For the  $\text{FPC}_{\text{AS}}$  and GPSR methods, we tune the regularization parameter  $\tau$  in (29) and select  $a = -6$ , see (28).

We compute an approximate log-likelihood function at *Iteration*  $p$  of the DORE and NIHT iterations as

$$\mathcal{L}^{(p)} = -0.5 N \ln \left( \frac{\|\mathbf{y} - H \mathbf{s}^{(p)}\|_2^2}{N} \right) \quad (36a)$$

obtained by taking the logarithm of (8), using the approximation  $H H^T \approx c I_N$  [see (10)], substituting  $\mathbf{s} = \mathbf{s}^{(p)}$ , and neglecting constant terms. Note that (36a) is a monotonic function of the residual squared error at *Iteration*  $p$ ; the residual squared error is a common measure for evaluating the performance of the NIHT algorithm. In Fig. 7, we show the approximate log likelihoods (36a) of the DORE and NIHT iterations for  $r \in \{5000, 20000\}$  as functions of CPU time and declare convergence at *Iteration*  $p$  satisfying  $|\mathcal{L}^{(p+1)} - \mathcal{L}^{(p)}| < 10^{-3}$ . For these two methods, we apply an approximate empirical Bayesian estimate of the random signal vector  $\mathbf{z}$ :

$$\hat{\mathbf{z}} = \mathbf{s}^{(+\infty)} + \frac{1}{c} H^T (\mathbf{y} - H \mathbf{s}^{(+\infty)}) \quad (36b)$$

obtained by substituting  $H H^T \approx c I_N$  into (16), see Figs. 5(c) and 6(c). Compared with ECME, DORE is also numerically robust when the approximation (10) is used: Even if the approximate ECME step fails to increase (36a) because of the inaccuracy of this approximation, the corresponding DORE step often succeeds. Indeed, in this example where we estimate  $c$  by averaging the diagonal elements of  $H H^T$ , the ECME iteration does not converge whereas DORE climbs the approximate log likelihood successfully, see Fig. 7.

For 180 uniform-angle projections, the FBP reconstruction is noisy compared with the DORE, NIHT, and  $\text{FPC}_{\text{AS}}$  sparse signal reconstructions, see Fig. 5. The GPSR reconstruction is noisy and also achieves a higher Lagrangian cost function (29) than  $\text{FPC}_{\text{AS}}$ .

For 160 limited-angle projections, the FBP reconstruction in Fig. 6 exhibits band artifacts caused by aliasing due to the missing projections. In contrast, DORE, NIHT, and  $\text{FPC}_{\text{AS}}$

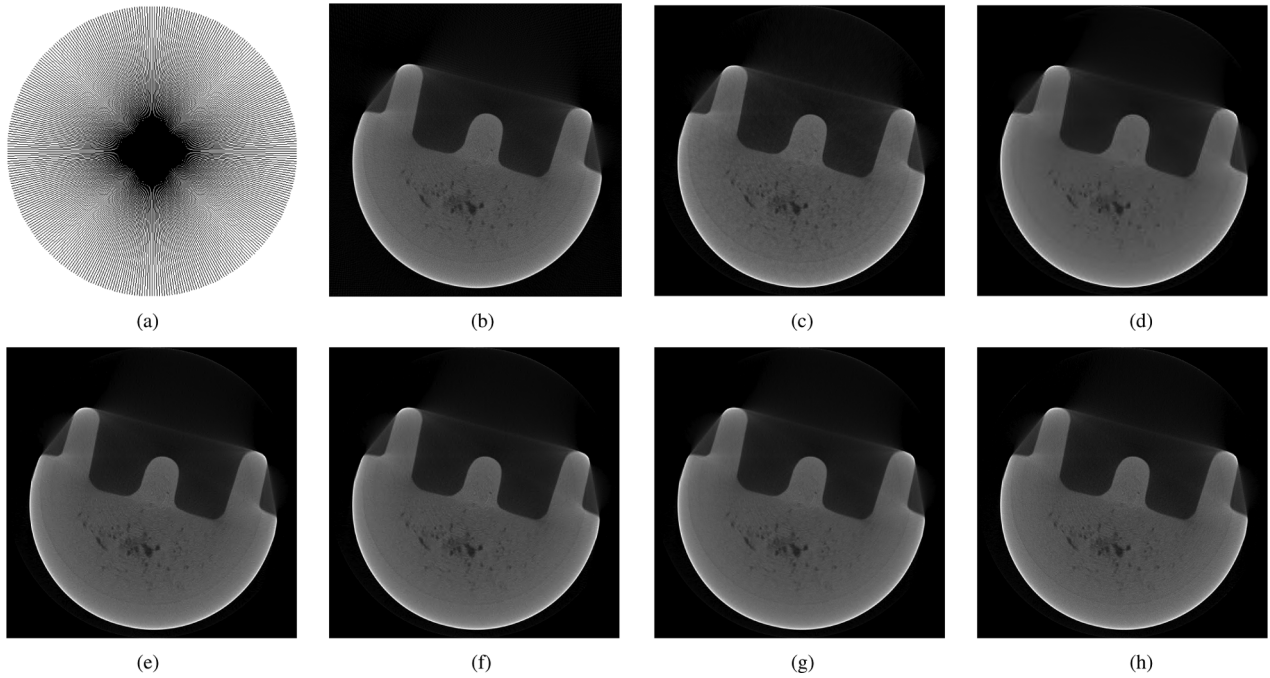


Fig. 5. (a) The frequency sampling pattern for 180 uniform-angle projections and (b)–(f) the corresponding reconstructions. (a) Sampling pattern. (b) FBP. (c) DORE with  $\hat{z}(r = 5000)$ . (d) DORE  $s^{(+\infty)}(r = 5000)$ . (e) DORE  $s^{(+\infty)}(r = 20000)$ . (f) NIHT  $s^{(+\infty)}(r = 20000)$ . (g) FPC<sub>AS,-6</sub>. (h) GPSR<sub>-6</sub>.

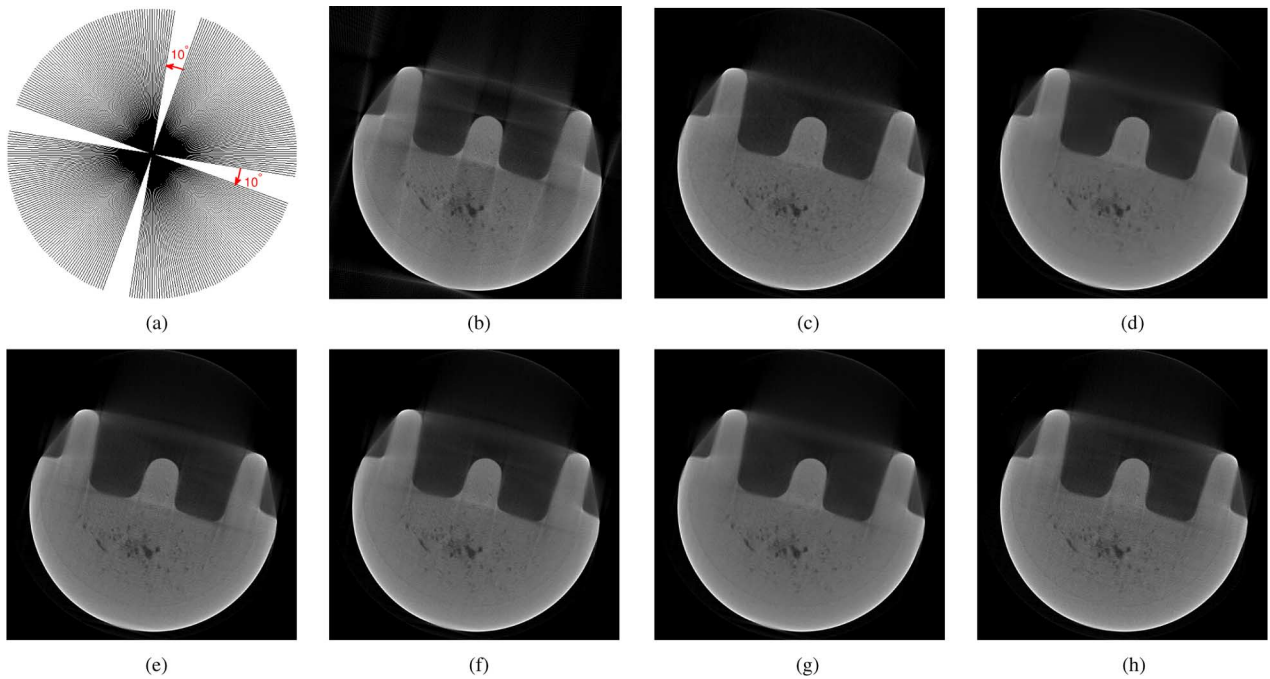


Fig. 6. (a) The frequency sampling pattern for 160 limited-angle projections and (b)–(f) the corresponding reconstructions. (a) Sampling pattern. (b) FBP. (c) DORE with  $\hat{z}(r = 5000)$ . (d) DORE  $s^{(+\infty)}(r = 5000)$ . (e) DORE  $s^{(+\infty)}(r = 20000)$ . (f) NIHT  $s^{(+\infty)}(r = 20000)$ . (g) FPC<sub>AS,-6</sub>. (h) GPSR<sub>-6</sub>.

yield reconstructions that are similar to those obtained from the full 180 uniform-angle projections: Compare parts (c)–(g) of Figs. 5 and 6. The GPSR reconstruction is noisy, has stronger band artifacts than the FPC<sub>AS</sub> reconstruction, and also achieves a higher Lagrangian cost function (29) than FPC<sub>AS</sub>.

Figs. 5(c) and 6(c) show the DORE reconstructions computed using  $\hat{z}$  in (36b) for  $r = 5000$  under the two sampling scenarios. Figs. 5(d)–(e) and 6(d)–(e) show the DORE recon-

structions computed using the sparse signal estimates  $\mathbf{s}^{(+\infty)}$  for  $r \in \{5000, 20000\}$  and Figs. 5(f) and 6(f) show the NIHT reconstructions computed using the sparse signal estimates  $\mathbf{s}^{(+\infty)}$  for  $r = 20000$ . For the same sparsity level  $r = 5000$ , the DORE and NIHT reconstructions based on  $\mathbf{s}^{(+\infty)}$  exhibit artifacts caused by the sparsifying transform and are blurred and smoother than the corresponding reconstructions based on  $\hat{z}$ . Selecting the larger sparsity level  $r = 20000$  removes the

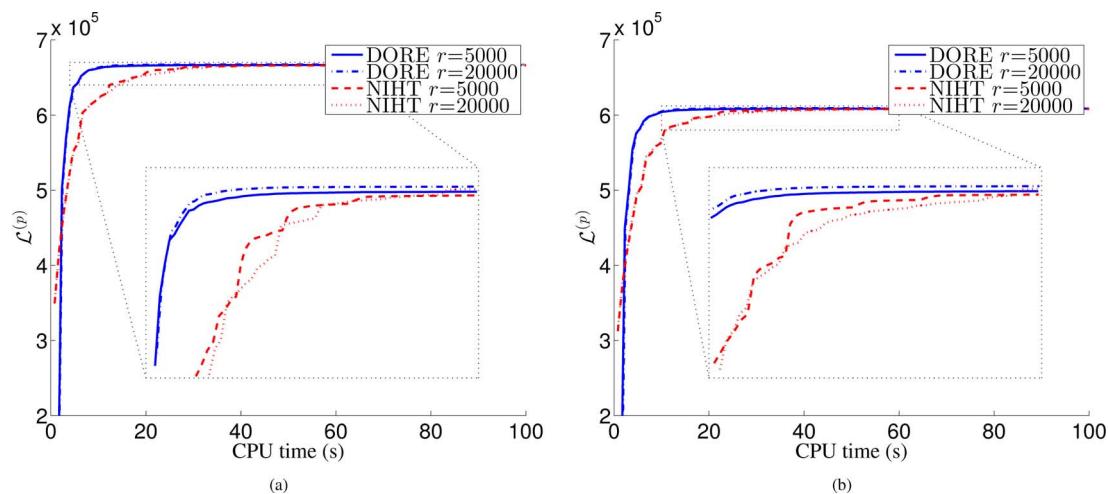


Fig. 7. The approximate log-likelihood function (36a) of the DORE and NIHT methods with  $r = 5000$  as a function of CPU time for (a) 180 uniform-angle projections and (b) 160 limited-angle projections.

TABLE I  
THE CPU TIMES OF VARIOUS METHODS IN SECONDS

	DORE ( $r = 5000$ )	NIHT ( $r = 5000$ )	DORE ( $r = 20000$ )	NIHT ( $r = 20000$ )	FPC <sub>AS,-6</sub>	GPSR <sub>-6</sub>
180 projections	99.1	3297.6	183.9	3606.5	1945.7	274.8
160 projections	362.1	4241.4	347.0	5001.1	1371.5	336.5

TABLE II  
THE APPROXIMATE LOG-LIKELIHOOD FUNCTIONS (36A) ACHIEVED UPON CONVERGENCE OF THE DORE AND NIHT ITERATIONS

	DORE ( $r = 5000$ )	NIHT ( $r = 5000$ )	DORE ( $r = 20000$ )	NIHT ( $r = 20000$ )
180 projections	666,575	666,466	667,317	667,249
160 projections	608,498	608,351	609,260	609,173

blurring, but also introduces scattered snow-like artifacts, see Figs. 5(e)–(f) and 6(e)–(f); in this case, the signal reconstruction based on  $\mathbf{s}^{(+\infty)}$  and  $\hat{\mathbf{z}}$  are almost identical and we show only those based on  $\mathbf{s}^{(+\infty)}$ .

Table I shows the CPU times of the compared sparse signal reconstruction methods. In this example, DORE is significantly faster than NIHT and FPC<sub>AS,-6</sub> and its speed is comparable to that of GPSR<sub>-6</sub> which, however, does not yield as good reconstructions as the other sparse reconstruction algorithms. Table II shows the convergence points of the log likelihoods in Fig. 7, i.e., the approximate log-likelihood function levels achieved by DORE and NIHT upon convergence.

## VII. CONCLUDING REMARKS

We proposed a probabilistic framework for sparse signal reconstruction and developed three hard thresholding methods based on this framework: ECME, DORE, and ADORE. ECME differs from the IHT algorithm by employing a stabilizing multiplicative term in each iteration step, which guarantees monotonic convergence for a wide range of sensing matrices. The DORE algorithm accelerates the convergence of the ECME iteration. We analyzed the convergence and reconstruction performances of the proposed ECME and DORE iterations. The conditions required by our theoretical analysis are invariant to

invertible linear transforms of the rows of the sensing matrix. In the large-scale applications where the multiplication by the stabilizing term is memory and computationally too expensive, an approximation is necessary. If we approximate the stabilizing term by a matrix proportional to identity, ECME reduces to IHT and the resulting approximate DORE algorithm can be viewed as a scheme for accelerating the IHT method. We proposed the tuning-free ADORE method based on our USS model selection criterion and showed the equivalence between USS and the  $(P_0)$  problem for sparse signals and noiseless measurements.

Further research will include incorporating information about the underlying signal structure and analyzing the reconstruction accuracy of the proposed algorithms.

## APPENDIX A ECME ALGORITHM DERIVATION

Consider the following hierarchical two-stage model:

$$p_{\mathbf{y}|\mathbf{z}}(\mathbf{y}|\mathbf{z}) = \mathcal{N}(\mathbf{y}; H\mathbf{z}, C) \quad (\text{A1a})$$

$$p_{\mathbf{z}|\boldsymbol{\theta}}(\mathbf{z}|\boldsymbol{\theta}) = \mathcal{N}(\mathbf{z}; \mathbf{s}, \sigma^2 I_m) \quad (\text{A1b})$$

where  $\mathbf{z}$  is the vector of missing data and  $C$  is a known noise covariance matrix. For  $C = 0_{N \times N}$ , this model reduces to that in (3a) and (3b) in Section II.

The *complete-data likelihood function* of the measurements  $\mathbf{y}$  and the missing data  $\mathbf{z}$  given  $\boldsymbol{\theta} = (\mathbf{s}, \sigma^2) \in \Theta_r$  follows from (A1a) and (A1b):

$$p_{\mathbf{z}, \mathbf{y} | \boldsymbol{\theta}}(\mathbf{z}, \mathbf{y} | \boldsymbol{\theta}) = \frac{\exp[-\frac{1}{2}(\mathbf{y} - H\mathbf{z})^T C^{-1}(\mathbf{y} - H\mathbf{z})]}{\sqrt{\det(2\pi C)}} \cdot \frac{\exp\left(-\frac{1}{2} \frac{\|\mathbf{z} - \mathbf{s}\|_2^2}{\sigma^2}\right)}{\sqrt{(2\pi\sigma^2)^m}}. \quad (\text{A2})$$

From (A2), the conditional pdf of  $\mathbf{z}$  given  $\mathbf{y}$  and  $\boldsymbol{\theta}$  is

$$p_{\mathbf{z} | \mathbf{y}, \boldsymbol{\theta}}(\mathbf{z} | \mathbf{y}, \boldsymbol{\theta}) = \mathcal{N}\left(\mathbf{z}; \mathbf{s} + \sigma^2 H^T (C + \sigma^2 H H^T)^{-1} \cdot (\mathbf{y} - H\mathbf{s}), \sigma^2 I_m - (\sigma^2)^2 H^T (C + \sigma^2 H H^T)^{-1} H\right) \quad (\text{A3})$$

see [32, Theorem 11.1]. Assume that the parameter estimate  $\boldsymbol{\theta}^{(p)} = (\mathbf{s}^{(p)}, (\sigma^2)^{(p)})$  is available; then, in *Iteration*  $p + 1$ , the E and M steps for estimating  $\mathbf{s}$  simplify to

$$\begin{aligned} \mathbf{z}^{(p+1)} &= E_{\mathbf{z} | \mathbf{y}, \boldsymbol{\theta}}[\mathbf{z} | \mathbf{y}, \boldsymbol{\theta}^{(p)}] \\ &= \mathbf{s}^{(p)} + (\sigma^2)^{(p)} H^T [C + (\sigma^2)^{(p)} H H^T]^{-1} \\ &\quad \cdot (\mathbf{y} - H\mathbf{s}^{(p)}) \end{aligned} \quad (\text{A4a})$$

and

$$\mathbf{s}^{(p+1)} = \arg \min_{\mathbf{s} \in \mathcal{S}_r} \|\mathbf{z}^{(p+1)} - \mathbf{s}\|_2^2 = \mathcal{T}_r(\mathbf{z}^{(p+1)}). \quad (\text{A4b})$$

Setting  $C = 0_{N \times N}$  in (A4a) and (A4b) yields (9a) and (9b), which are not dependent on  $(\sigma^2)^{(p)}$ .

## APPENDIX B

### USS( $r$ ) AS AN APPROXIMATE GML CRITERION

For a given signal support set  $A = \text{supp}(\mathbf{s})$  with  $\dim(A) = r$ , the FIM for the nonzero signal coefficients  $\mathbf{s}_A$  and the variance parameter  $\sigma^2$  is given by

$$\mathcal{I}(\boldsymbol{\theta}) = \frac{1}{\sigma^2} \begin{bmatrix} H_A^T (H H^T)^{-1} H_A & \mathbf{0}_r \\ \mathbf{0}_r^T & \frac{1}{2} \frac{N}{\sigma^2} \end{bmatrix} \quad (\text{B1})$$

which follows using the FIM result for the Gaussian measurement model [32, eq. (3.32) on p. 48]. Substituting (6a) and (B1) into (19) yields

$$\begin{aligned} \text{GML}(r) &= \text{const} - \frac{1}{2} N \ln[\hat{\sigma}_{\text{ML}}^2(r)] \\ &\quad - \frac{1}{2} \left\{ -(r+2) \ln[\hat{\sigma}_{\text{ML}}^2(r)] \right. \\ &\quad \left. + \ln[\det(H_A^T (H H^T)^{-1} H_A)] \right\} \end{aligned} \quad (\text{B2a})$$

$$\begin{aligned} &\approx \text{const} - \frac{1}{2} (N - r - 2) \ln[\hat{\sigma}_{\text{ML}}^2(r)] \\ &\quad - \frac{1}{2} r \ln\left(\frac{N}{m}\right) \end{aligned} \quad (\text{B2b})$$

where  $\text{const}$  corresponds to the terms that are not functions of  $r$  and  $\hat{A} = \text{supp}(\hat{\mathbf{s}}_{\text{ML}}(r))$ . In (B2b), we approximate the computationally expensive term  $\ln[\det(H_A^T (H H^T)^{-1} H_A)]$

by  $r \ln\left(\frac{N}{m}\right)$ , which is a quite good approximation when  $H$  is a random Gaussian or Bernoulli matrix.

Since  $\text{GML}(r)$  and its approximation in (19) and (B2b) are *not scale-invariant*, i.e., it is affected by scaling of the measurement vector  $\mathbf{y}$  by a nonzero constant, we *normalize*  $\mathbf{y}$  so that  $\frac{\mathbf{y}^T (H H^T)^{-1} \mathbf{y}}{N} = 1$ , leading to the *scale-invariant* USS criterion in (17).

## APPENDIX C

### PROOF OF EQUIVALENCE BETWEEN USS AND THE ( $P_0$ ) PROBLEM (1)

*Proof of Theorem 1:* When conditions (1) and (2) of Theorem 1 hold, we have  $\text{spark}(H) = N + 1 > 2r^\diamond$  and the condition of [8, Theorem 2] is satisfied. Therefore,  $\mathbf{s}^\diamond$  is the unique solution of the ( $P_0$ ) problem, according to [8, Theorem 2]. We now consider the USS function under different sparsity level  $r$ .

For  $r = r^\diamond$ , the ML estimate of  $\boldsymbol{\theta}$  is  $\hat{\boldsymbol{\theta}}_{\text{ML}}(r^\diamond) = (\hat{\mathbf{s}}_{\text{ML}}(r^\diamond), \hat{\sigma}_{\text{ML}}^2(r^\diamond)) = (\mathbf{s}^\diamond, 0)$  and unique, since it leads to infinite likelihood function (6a) and no other  $\boldsymbol{\theta}$  yields infinite likelihood, due to the fact that  $\mathbf{s}^\diamond$  is the unique solution of the ( $P_0$ ) problem. Plugging  $\hat{\sigma}_{\text{ML}}^2(r^\diamond) = 0$  into (17) yields

$$\text{USS}(r^\diamond) = -\frac{1}{2} r^\diamond \ln\left(\frac{N}{m}\right) - \frac{1}{2} (N - r^\diamond - 2) \ln \varepsilon. \quad (\text{C1})$$

Furthermore, since (20b) holds, we have  $N - r^\diamond - 2 > 0$  and therefore  $\text{USS}(r)$  grows to positive infinity as  $\varepsilon$  decreases to zero.

For  $r < r^\diamond$ ,  $\mathbf{y} \neq H\mathbf{s}$  for any  $r$ -sparse vector  $\mathbf{s}$ ; consequently,  $\sigma_{\text{ML}}^2(r) > 0$  and  $\text{USS}(r)$  is finite. As long as we pick a sufficiently small  $\varepsilon > 0$ ,  $\text{USS}(r)$  for  $r < r^\diamond$  will be always smaller than  $\text{USS}(r^\diamond)$ .

For  $r > r^\diamond$ , the ML estimate of  $\sigma^2$  must be  $\hat{\sigma}_{\text{ML}}^2(r) = 0$ , which leads to infinite likelihood. However, in this case, we have

$$\begin{aligned} \text{USS}(r) - \text{USS}(r^\diamond) &= -\frac{1}{2} (r - r^\diamond) \ln\left(\frac{N}{m}\right) \\ &\quad + \frac{1}{2} (r - r^\diamond) \ln \varepsilon < 0 \end{aligned} \quad (\text{C2})$$

for small enough  $\varepsilon > 0$ .

The claim follows by combining the above conclusions.  $\square$

## APPENDIX D

### PROOFS OF THE CONVERGENCE RESULTS IN SECTION V

To prove Theorem 2, we first need the following lemmas.

*Lemma 1:* Assume that the sensing matrix  $H$  satisfies the URP condition, see also (20a). For an index set  $A \subset \{1, 2, \dots, m\}$ , if

$$0 < \dim(A) \leq m - N \quad (\text{D1a})$$

then

$$\lambda_{\max}(H_A^T (H H^T)^{-1} H_A) < 1. \quad (\text{D1b})$$

*Proof:* Observe that

$$\begin{aligned} & \lambda_{\max}(H_A^T (H H^T)^{-1} H_A) \\ &= \lambda_{\max}((H H^T)^{-1} H_A H_A^T) \\ &= \lambda_{\max}(I_N - (H H^T)^{-1} H_{A^c} H_{A^c}^T) \end{aligned} \quad (D2)$$

where

$$A^c \triangleq \{1, 2, \dots, m\} \setminus A \quad (D3)$$

defines the index set complementary to  $A$ . By (D1a),  $\dim(A^c) = m - \dim(A) \geq N$ . And, due to the URP condition,  $H_{A^c} H_{A^c}^T$  is full rank. Combining these facts, we conclude that  $(H H^T)^{-1} H_{A^c} H_{A^c}^T$  is strictly positive definite; therefore,

$$\begin{aligned} & \lambda_{\max}(H_A^T (H H^T)^{-1} H_A) \\ &= 1 - \lambda_{\min}((H H^T)^{-1} H_{A^c} H_{A^c}^T) < 1 \end{aligned} \quad (D4)$$

and (D1b) follows.  $\square$

Lemma 1 leads to the following result which is useful for the proof of Theorem 2.

*Lemma 2:* Under the conditions of Theorem 2, the distance between two consecutive ECME signal iterates  $\|\mathbf{s}^{(p+1)} - \mathbf{s}^{(p)}\|_2$  goes to zero. Similarly, the distance between two consecutive DORE signal iterates also  $\|\mathbf{s}^{(p+1)} - \mathbf{s}^{(p)}\|_2$  goes to zero.

*Proof:* We first prove the lemma for the ECME iteration. Let  $\mathbf{s}^{(p)}$  and  $\mathbf{s}^{(p+1)}$  be ECME signal updates at Iterations  $p$  and  $p+1$ , respectively. If  $\mathbf{s}^{(p+1)} = \mathbf{s}^{(p)}$ , the lemma immediately follows. Therefore, without loss of generality, we assume  $\mathbf{s}^{(p+1)} \neq \mathbf{s}^{(p)}$ . Since  $\mathcal{E}(\mathbf{s}^{(p)})$  in (21) converges to a limit,  $\mathcal{E}(\mathbf{s}^{(p)}) - \mathcal{E}(\mathbf{s}^{(p+1)})$  converges to zero. Now,

$$\begin{aligned} & \mathcal{E}(\mathbf{s}^{(p)}) - \mathcal{E}(\mathbf{s}^{(p+1)}) \\ &= \mathcal{Q}(\mathbf{s}^{(p)} | \mathbf{s}^{(p)}) - \mathcal{H}(\mathbf{s}^{(p)} | \mathbf{s}^{(p)}) \\ &\quad - [\mathcal{Q}(\mathbf{s}^{(p+1)} | \mathbf{s}^{(p)}) - \mathcal{H}(\mathbf{s}^{(p+1)} | \mathbf{s}^{(p)})] \end{aligned} \quad (D5a)$$

$$\begin{aligned} & \geq (\mathbf{s}^{(p+1)} - \mathbf{s}^{(p)})^T [I_m - H^T (H H^T)^{-1} H] \\ &\quad \cdot (\mathbf{s}^{(p+1)} - \mathbf{s}^{(p)}) \end{aligned} \quad (D5b)$$

$$\begin{aligned} &= (\mathbf{s}_A^{(p+1)} - \mathbf{s}_A^{(p)})^T \cdot [J_{\dim(A)} - H_A^T (H H^T)^{-1} H_A] \\ &\quad \cdot (\mathbf{s}_A^{(p+1)} - \mathbf{s}_A^{(p)}) \end{aligned} \quad (D5c)$$

$$\begin{aligned} &= \left[ 1 - \frac{1}{\|\mathbf{s}^{(p+1)} - \mathbf{s}^{(p)}\|_2^2} (\mathbf{s}_A^{(p+1)} - \mathbf{s}_A^{(p)})^T \right. \\ &\quad \cdot H_A^T (H H^T)^{-1} H_A (\mathbf{s}_A^{(p+1)} - \mathbf{s}_A^{(p)}) \left. \right] \\ &\quad \cdot \|\mathbf{s}^{(p+1)} - \mathbf{s}^{(p)}\|_2^2 \end{aligned} \quad (D5d)$$

$$\begin{aligned} & \geq \left[ 1 - \lambda_{\max}(H_A^T (H H^T)^{-1} H_A) \right] \\ &\quad \cdot \|\mathbf{s}^{(p+1)} - \mathbf{s}^{(p)}\|_2^2 \end{aligned} \quad (D5e)$$

where  $A = \text{supp}(\mathbf{s}^{(p)}) \cup \text{supp}(\mathbf{s}^{(p+1)})$ . Here, (D5a) follows from (22a), (D5b) follows by (23a) and the fact that  $\mathcal{H}(\mathbf{s}^{(p)} | \mathbf{s}^{(p)}) = 0$ , (D5c) is obtained by using the identities  $\|\mathbf{s}^{(p+1)} - \mathbf{s}^{(p)}\|_2^2 = \|\mathbf{s}_A^{(p+1)} - \mathbf{s}_A^{(p)}\|_2^2$  and  $H(\mathbf{s}^{(p+1)} - \mathbf{s}^{(p)}) = H_A(\mathbf{s}_A^{(p+1)} - \mathbf{s}_A^{(p)})$ , and (D5e) follows by using the Rayleigh-quotient property [44, Theorem 21.5.6]. Note that  $0 < \dim(A) \leq 2r \leq m - N$ , where the second inequality follows from (26). Therefore, (D1a) holds and (D1b) in Lemma 1 implies that the term  $1 - \lambda_{\max}(H_A^T (H H^T)^{-1} H_A)$

in (D5e) is strictly positive. Since  $\mathcal{E}(\mathbf{s}^{(p)}) - \mathcal{E}(\mathbf{s}^{(p+1)})$  converges to zero, then  $\|\mathbf{s}^{(p+1)} - \mathbf{s}^{(p)}\|_2^2$  converges to zero as well. This completes the proof for the ECME iteration.

Now, let  $\mathbf{s}^{(p)}$  and  $\mathbf{s}^{(p+1)}$  be DORE signal updates at DORE Iterations  $p$  and  $p+1$ , respectively, and let the  $\hat{\mathbf{s}}$  be the ECME signal update in Step 1 of DORE Iteration  $p+1$ . Step 5 of the DORE scheme ensures  $\mathcal{E}(\mathbf{s}^{(p+1)}) \leq \mathcal{E}(\hat{\mathbf{s}})$  and, therefore,

$$\mathcal{E}(\mathbf{s}^{(p)}) - \mathcal{E}(\mathbf{s}^{(p+1)}) \geq \mathcal{E}(\mathbf{s}^{(p)}) - \mathcal{E}(\hat{\mathbf{s}}) \quad (D6a)$$

$$\begin{aligned} & \geq \left[ 1 - \lambda_{\max}(H_A^T (H H^T)^{-1} H_A) \right] \\ &\quad \cdot \|\hat{\mathbf{s}} - \mathbf{s}^{(p)}\|_2^2 \end{aligned} \quad (D6b)$$

where  $A = \text{supp}(\mathbf{s}^{(p)}) \cup \text{supp}(\hat{\mathbf{s}})$ , and (D6b) follows from (D5). By the discussion in Section V prior to Theorem 2, for DORE estimates  $\mathbf{s}^{(p)}$ , we have  $\mathcal{E}(\mathbf{s}^{(p)})$  converges to a limit, and  $\mathcal{E}(\mathbf{s}^{(p)}) - \mathcal{E}(\mathbf{s}^{(p+1)})$  converges to zero. Therefore, mimicking the arguments for ECME convergence, we have  $\|\hat{\mathbf{s}} - \mathbf{s}^{(p)}\|_2^2$  converges to zero as well. This concludes the proof of Lemma 2.  $\square$

The following two lemmas are also needed for the proof of Theorem 2.

*Lemma 3:* For any  $r$ -sparse vector  $\mathbf{s}' \in \mathcal{S}_r$ , there exists a  $\delta > 0$  such that, for all  $\mathbf{s} \in \mathcal{S}_r$  satisfying  $\|\mathbf{s} - \mathbf{s}'\|_2 < \delta$ , we have

$$\dim(\text{supp}(\mathbf{s}) \cup \text{supp}(\mathbf{s}')) \leq r. \quad (D7)$$

*Proof:* The proof is by contradiction. First, define  $A = \text{supp}(\mathbf{s})$  and  $A' = \text{supp}(\mathbf{s}')$ . Suppose that, for all  $\delta > 0$ , there exists a  $\mathbf{s} \in \mathcal{S}_r$  satisfying  $\|\mathbf{s} - \mathbf{s}'\|_2 < \delta$  and  $\dim(A \cup A') > r$ . Since  $\dim(A) \leq r$ ,

$$\dim(A' \cap A^c) = \dim(A \cup A') - \dim(A) > r - r = 0 \quad (D8)$$

implying that the set  $A' \cap A^c$  is not empty, see also the definition of the complementary index set in (D3). Choose  $\delta$  to be half the magnitude of the smallest nonzero element in  $\mathbf{s}'$ :  $\delta = \frac{1}{2} \min_{i \in A'} |s'_i|$ . Now,

$$\|\mathbf{s} - \mathbf{s}'\|_2 \geq \|\mathbf{s}'_{A' \cap A^c}\|_2 \geq \min_{i \in A'} |s'_i| > \delta \quad (D9)$$

which contradicts to the assumption that  $\|\mathbf{s} - \mathbf{s}'\|_2 < \delta$  for all  $\delta > 0$ . Therefore, Lemma 3 follows.  $\square$

*Lemma 4:* An  $r$ -sparse vector  $\mathbf{s}^* \in \mathcal{S}_r$  is an  $r$ -local maximum or minimum of a twice differentiable function  $f(\mathbf{s}) : \mathbb{R}^m \rightarrow \mathbb{R}$  if

- (1) for all  $i \in \{1, 2, \dots, m\}$  such that

$$\dim(\{i\} \cup \text{supp}(\mathbf{s}^*)) \leq r \quad (D10a)$$

we have

$$\frac{\partial f(\mathbf{s})}{\partial s_i} \Big|_{\mathbf{s}=\mathbf{s}^*} = \mathbf{0}_{m \times 1} \quad (D10b)$$

and

- (2) there exists a  $\delta > 0$ , such that, for all  $\mathbf{s} \in \mathcal{S}_r$  satisfying  $\|\mathbf{s} - \mathbf{s}^*\|_2 < \delta$ , the Hessian matrix

$$\frac{\partial^2 f(\mathbf{s})}{\partial \mathbf{s} \partial \mathbf{s}^T} \quad (D11)$$

is negative semidefinite (for a maximum) or positive semidefinite (for a minimum).

*Proof:* We first consider the case of an  $r$ -local maximum of  $f(\mathbf{s})$  and assume that conditions (1) and (2) hold for a point  $\mathbf{s}^* \in \mathcal{S}_r$ . By condition (2), for the positive number  $\delta_1$ , the Hessian matrix is negative semidefinite around  $\mathbf{s}^*$  for all  $\mathbf{s} \in \mathcal{S}_r$  satisfying  $\|\mathbf{s} - \mathbf{s}^*\|_2 < \delta_1$ . By Lemma 3, for any  $r$ -sparse vector  $\mathbf{s}^*$ , there exists a  $\delta_2 > 0$  such that, for all  $\mathbf{s} \in \mathcal{S}_r$  satisfying  $\|\mathbf{s} - \mathbf{s}^*\|_2 < \delta_2$ , we have

$$\dim(\text{supp}(\mathbf{s}) \cup \text{supp}(\mathbf{s}^*)) \leq r. \quad (\text{D12})$$

Now, for  $\delta = \min\{\delta_1, \delta_2\}$ , consider any  $\mathbf{s} \in \mathcal{S}_r$  satisfying  $\|\mathbf{s} - \mathbf{s}^*\|_2 < \delta$ , and expand  $f(\mathbf{s})$  around  $\mathbf{s}^*$  using the Taylor series with Lagrange's form of the remainder [45, p. 243]:

$$\begin{aligned} f(\mathbf{s}) - f(\mathbf{s}^*) &= (\mathbf{s} - \mathbf{s}^*)^T \frac{\partial f(\mathbf{s})}{\partial \mathbf{s}} \Big|_{\mathbf{s}=\mathbf{s}^*} \\ &\quad + \frac{1}{2} (\mathbf{s} - \mathbf{s}^*)^T \frac{\partial^2 f(\mathbf{s})}{\partial \mathbf{s} \partial \mathbf{s}^T} \Big|_{\mathbf{s}=\mathbf{s}^* + c(\mathbf{s} - \mathbf{s}^*)} (\mathbf{s} - \mathbf{s}^*) \end{aligned} \quad (\text{D13a})$$

$$\leq (\mathbf{s} - \mathbf{s}^*)^T \frac{\partial f(\mathbf{s})}{\partial \mathbf{s}} \Big|_{\mathbf{s}=\mathbf{s}^*} \quad (\text{D13b})$$

$$= \sum_{i \in \text{supp}(\mathbf{s}) \cup \text{supp}(\mathbf{s}^*)} (\mathbf{s}_i - \mathbf{s}_i^*) \frac{\partial f(\mathbf{s})}{\partial s_i} \Big|_{\mathbf{s}=\mathbf{s}^*} \quad (\text{D13c})$$

$$= 0 \quad (\text{D13d})$$

where  $c \in (0, 1)$ . Since the vector  $\mathbf{s}^* + c(\mathbf{s} - \mathbf{s}^*)$  is  $r$ -sparse and satisfies  $\|\mathbf{s}^* + c(\mathbf{s} - \mathbf{s}^*) - \mathbf{s}^*\|_2 < \delta$ , the Hessian in (D13a) is negative-semidefinite and (D13b) follows. Condition (1) of Lemma 4 and (D12) imply that the partial derivatives in (D10b) are zero for all coordinates with indices  $i \in \text{supp}(\mathbf{s}) \cup \text{supp}(\mathbf{s}^*)$ , and (D13d) follows. Now, we have a  $\delta = \min\{\delta_1, \delta_2\} > 0$  such that, for all  $\mathbf{s} \in \mathcal{S}_r$  satisfying  $\|\mathbf{s} - \mathbf{s}^*\|_2 < \delta$ ,  $f(\mathbf{s}) \leq f(\mathbf{s}^*)$ ; therefore  $\mathbf{s}^*$  is an  $r$ -local maximum.

If the Hessian matrix  $\frac{\partial^2 f(\mathbf{s})}{\partial \mathbf{s} \partial \mathbf{s}^T}$  is positive semidefinite around  $\mathbf{s}^*$ , then  $\frac{\partial^2 [-f(\mathbf{s})]}{\partial \mathbf{s} \partial \mathbf{s}^T}$  is negative semidefinite around  $\mathbf{s}^*$ . Therefore,  $\mathbf{s}^*$  is an  $r$ -local maximum of  $-f(\mathbf{s})$ , and, by Definition 1,  $\mathbf{s}^*$  is an  $r$ -local minimum of  $f(\mathbf{s})$ .  $\square$

Lemma 4 gives a sufficient condition for checking an  $r$ -local maximum or minimum point. The first condition of Lemma 4 implies that, instead of checking that all partial derivatives of our function are zero (which is required in the standard first-derivative test for finding local maxima and minima), we only need to check its derivatives along a few *allowed* coordinate axes, where the allowed coordinate axes are defined by the property that perturbing along these axes does not violate the sparsity requirement, see (D10a). If  $\mathbf{s}^*$  has exactly  $r$  nonzero elements, then  $i$  in (D10a) must be in  $\text{supp}(\mathbf{s}^*)$ , and we should only check the  $r$  partial derivatives that correspond to the nonzero components of  $\mathbf{s}^*$ .

We are now ready to show Theorem 2.

*Proof of Theorem:* We first prove the Theorem for the ECME iteration. Let  $\mathbf{s}^{(p)}$  and  $\mathbf{s}^{(p+1)}$  be ECME signal updates at Iterations  $p$  and  $p + 1$ , respectively. Now, we have

$$\begin{aligned} \mathbf{s}^{(p+1)} &= \arg \min_{\mathbf{s} \in \mathcal{S}_r} \mathcal{Q}(\mathbf{s} | \mathbf{s}^{(p)}) \\ &= \arg \min_{\mathbf{s} \in \mathcal{S}_r} \|\mathbf{s} - [\mathbf{s}^{(p)} + H^T (HH^T)^{-1} (\mathbf{y} - H\mathbf{s}^{(p)})]\|_2^2 \end{aligned} \quad (\text{D14})$$

see (9b) and (22b). By Lemma 2,  $\|\mathbf{s}^{(p+1)} - \mathbf{s}^{(p)}\|_2^2$  goes to zero as  $p$  grows.

We first show that the conditions of Lemma 4 hold for the function  $f(\mathbf{s}) = \mathcal{E}(\mathbf{s})$  in (21) and the  $r$ -sparse vector  $\mathbf{s}^{(p+1)}$  as  $p$  goes to infinity. The proof is by contradiction. Suppose that condition (1) of Lemma 4 is not satisfied as  $p$  goes to infinity, i.e.,

$$\max_{j: \dim(\{j\} \cup \text{supp}(\mathbf{s}^{(p+1)})) \leq r} \left| \frac{\partial \mathcal{E}(\mathbf{s}^{(p+1)})}{\partial s_j} \right| \geq a > 0 \quad (\text{D15})$$

as  $p$  goes to infinity. Here,  $a$  is some strictly positive constant and

$$\frac{\partial \mathcal{E}(\mathbf{s}^{(p+1)})}{\partial s_j} \triangleq \frac{\partial \mathcal{E}(\mathbf{s})}{\partial s_j} \Big|_{\mathbf{s}=\mathbf{s}^{(p+1)}}. \quad (\text{D16})$$

Let

$$i^{(p+1)} = \arg \max_{j: \dim(\{j\} \cup \text{supp}(\mathbf{s}^{(p+1)})) \leq r} \left| \frac{\partial \mathcal{E}(\mathbf{s}^{(p+1)})}{\partial s_j} \right| \quad (\text{D17})$$

and for simplicity of notation, we just write  $i = i^{(p+1)}$ . Without loss of generality, assume that this partial derivative is strictly positive:  $\frac{\partial \mathcal{E}(\mathbf{s}^{(p+1)})}{\partial s_i} > 0$ . By the definitions of the partial derivative and limit, for the real number  $\frac{1}{2} \frac{\partial \mathcal{E}(\mathbf{s}^{(p+1)})}{\partial s_i}$ , there exists a positive number  $\delta > 0$  such that, for all  $\epsilon \in (0, \delta)$ , the vector  $\mathbf{s}_\epsilon = \mathbf{s}^{(p+1)} - \epsilon \mathbf{e}_i$  satisfies

$$\begin{aligned} \left| \frac{\mathcal{E}(\mathbf{s}^{(p+1)} - \epsilon \mathbf{e}_i) - \mathcal{E}(\mathbf{s}^{(p+1)})}{-\epsilon} - \frac{\partial \mathcal{E}(\mathbf{s}^{(p+1)})}{\partial s_i} \right| \\ < \frac{1}{2} \frac{\partial \mathcal{E}(\mathbf{s}^{(p+1)})}{\partial s_i} \end{aligned} \quad (\text{D18a})$$

and, therefore,

$$\begin{aligned} \mathcal{E}(\mathbf{s}^{(p+1)} - \epsilon \mathbf{e}_i) &< \mathcal{E}(\mathbf{s}^{(p+1)}) - \frac{1}{2} \epsilon \frac{\partial \mathcal{E}(\mathbf{s}^{(p+1)})}{\partial s_i} \\ &\leq \mathcal{E}(\mathbf{s}^{(p+1)}) - \frac{1}{2} \epsilon a. \end{aligned} \quad (\text{D18b})$$

Now, compute [see (22c)]

$$\begin{aligned} &\mathcal{H}(\mathbf{s}^{(p+1)} - \epsilon \mathbf{e}_i | \mathbf{s}^{(p)}) - \mathcal{H}(\mathbf{s}^{(p+1)} | \mathbf{s}^{(p)}) \\ &= (\mathbf{s}^{(p+1)} - \epsilon \mathbf{e}_i - \mathbf{s}^{(p)})^T \\ &\quad \cdot [I_m - H^T (HH^T)^{-1} H] (\mathbf{s}^{(p+1)} - \epsilon \mathbf{e}_i - \mathbf{s}^{(p)}) \\ &\quad - (\mathbf{s}^{(p+1)} - \mathbf{s}^{(p)})^T \\ &\quad \cdot [I_m - H^T (HH^T)^{-1} H] (\mathbf{s}^{(p+1)} - \mathbf{s}^{(p)}) \quad (\text{D19a}) \\ &\leq (\mathbf{s}^{(p+1)} - \epsilon \mathbf{e}_i - \mathbf{s}^{(p)})^T \\ &\quad \cdot [I_m - H^T (HH^T)^{-1} H] (\mathbf{s}^{(p+1)} - \epsilon \mathbf{e}_i - \mathbf{s}^{(p)}) \end{aligned} \quad (\text{D19b})$$

$$\leq \|\mathbf{s}^{(p+1)} - \epsilon \mathbf{e}_i - \mathbf{s}^{(p)}\|_2^2 \quad (\text{D19c})$$

$$\leq (\|\mathbf{s}^{(p+1)} - \mathbf{s}^{(p)}\|_2 + \epsilon)^2 \quad (\text{D19d})$$

where (D19c) follows by observing that  $H^T (HH^T)^{-1} H$  is positive semidefinite and (D19d) holds due to the triangle inequality.

Therefore, we have [see (22a)]

$$\begin{aligned} \mathcal{Q}(\mathbf{s}^{(p+1)} - \epsilon \mathbf{e}_i | \mathbf{s}^{(p)}) &= \mathcal{E}(\mathbf{s}^{(p+1)} - \epsilon \mathbf{e}_i) + \mathcal{H}(\mathbf{s}^{(p+1)} - \epsilon \mathbf{e}_i | \mathbf{s}^{(p)}) \quad (\text{D20a}) \\ &< \mathcal{E}(\mathbf{s}^{(p+1)}) - \frac{1}{2} \epsilon a + \mathcal{H}(\mathbf{s}^{(p+1)} | \mathbf{s}^{(p)}) \\ &\quad + (\|\mathbf{s}^{(p+1)} - \mathbf{s}^{(p)}\|_2 + \epsilon)^2 \quad (\text{D20b}) \\ &= \mathcal{Q}(\mathbf{s}^{(p+1)} | \mathbf{s}^{(p)}) - \left(\frac{1}{2}a - \epsilon\right) \epsilon \\ &\quad + \|\mathbf{s}^{(p+1)} - \mathbf{s}^{(p)}\|_2^2 \\ &\quad + 2\epsilon \|\mathbf{s}^{(p+1)} - \mathbf{s}^{(p)}\|_2 \quad (\text{D20c}) \end{aligned}$$

where (D20b) follows from (D18b) and (D19). Note that the terms  $\|\mathbf{s}^{(p+1)} - \mathbf{s}^{(p)}\|_2^2 + 2\epsilon \|\mathbf{s}^{(p+1)} - \mathbf{s}^{(p)}\|_2$  converges to zero as  $p$  grows according to Lemma 2. Observe also that the vector  $\mathbf{s}_\epsilon = \mathbf{s}^{(p+1)} - \epsilon \mathbf{e}_i$  is  $r$ -sparse. So, for any

$$\epsilon \in \left(0, \min\left\{\delta, \frac{1}{2}a\right\}\right) \quad (\text{D21})$$

we have  $\mathcal{Q}(\mathbf{s}_\epsilon | \mathbf{s}^{(p)}) < \mathcal{Q}(\mathbf{s}^{(p+1)} | \mathbf{s}^{(p)})$  (as  $p$  goes to infinity), which contradicts to (D14). Hence, the condition (1) of Lemma 4 holds as  $p$  grows to infinity.

The condition (2) of Lemma 4 holds because, for any  $\mathbf{s} \in \mathbb{R}^m$ , the Hessian of  $\mathcal{E}(\mathbf{s})$  is  $2H^T(HH^T)^{-1}H$  which is clearly a positive semidefinite matrix.

Since the conditions of Lemma 4 hold for the function  $f(\mathbf{s}) = \mathcal{E}(\mathbf{s})$  in (21) and  $\mathbf{s}^{(p+1)}$  (as  $p$  goes to infinity), we apply Lemma 4 and conclude that  $\mathbf{s}^{(p)}$  converges to an  $r$ -local minimum point of  $\mathcal{E}(\mathbf{s})$  and consequently an  $r$ -local maximum point of the concentrated marginal likelihood function (8), which follows from the fact that (8) is a monotonically decreasing function of  $\mathcal{E}(\mathbf{s}) = N\hat{\sigma}^2(\mathbf{s})$ , see also (7).

Now, for DORE iteration, let  $\mathbf{s}^{(p)}$  be DORE signal update at DORE Iterations  $p$ , and let the  $\hat{\mathbf{s}}$  be the ECME signal update in Step 1 of DORE Iteration  $p + 1$ :

$$\begin{aligned} \hat{\mathbf{s}} &= \arg \min_{\mathbf{s} \in \mathcal{S}_r} \mathcal{Q}(\mathbf{s} | \mathbf{s}^{(p)}) \\ &= \arg \min_{\mathbf{s} \in \mathcal{S}_r} \|\mathbf{s} - [\mathbf{s}^{(p)} + H^T(HH^T)^{-1}(\mathbf{y} - H\mathbf{s}^{(p)})]\|_2^2 \quad (\text{D22}) \end{aligned}$$

and according to (D6),  $\|\hat{\mathbf{s}} - \mathbf{s}^{(p)}\|_2^2$  converges to zero. Simply apply the same arguments from (D14)–(D20) for ECME to DORE by replacing  $\mathbf{s}^{(p+1)}$  with  $\hat{\mathbf{s}}$ , and we conclude that the DORE signal iterate also converges to an  $r$ -local maximum point of the concentrated marginal likelihood function (8).  $\square$

#### ACKNOWLEDGMENT

The authors are grateful to Dr. J. N. Gray, Center for Nondestructive Evaluation, Iowa State University, for providing real X-ray CT data used in the numerical example in Section VI-C and R. Gu, Electrical and Computer Engineering, Iowa State University, for preparing some of the experimental results in Section VI-C.

#### REFERENCES

- [1] M. Lustig, D. Donoho, and J. Pauly, "Sparse MRI: The application of compressed sensing for rapid MR imaging," *Magn. Reson. Med.*, vol. 58, pp. 1182–1195, Dec. 2007.
- [2] W. Bajwa, J. Haupt, A. Sayeed, and R. Nowak, "Joint source-channel communication for distributed estimation in sensor networks," *IEEE Trans. Inf. Theory*, vol. 53, no. 10, pp. 3629–3653, Oct. 2007.
- [3] I. F. Gorodnitsky and B. D. Rao, "Sparse signal reconstruction from limited data using FOCUSS: A re-weighted minimum norm algorithm," *IEEE Trans. Signal Process.*, vol. 45, pp. 600–616, Mar. 1997.
- [4] E. J. Candès, J. Romberg, and T. Tao, "Robust uncertainty principles: Exact signal reconstruction from highly incomplete frequency information," *IEEE Trans. Inf. Theory*, vol. 52, no. 2, pp. 489–509, 2006.
- [5] E. J. Candès and T. Tao, "Decoding by linear programming," *IEEE Trans. Inf. Theory*, vol. 51, pp. 4203–4215, Dec. 2005.
- [6] R. G. Baraniuk, "Compressive sensing," *IEEE Signal Process. Mag.*, vol. 24, pp. 118–121, Jul. 2007.
- [7] *IEEE Signal Process. Mag. (Special Issue on Compressive Sampling)*, vol. 25, no. 2, Mar. 2008.
- [8] A. M. Bruckstein, D. L. Donoho, and M. Elad, "From sparse solutions of systems of equations to sparse modeling of signals and images," *SIAM Rev.*, vol. 51, pp. 34–81, Mar. 2009.
- [9] B. K. Natarajan, "Sparse approximate solutions to linear systems," *SIAM J. Comput.*, vol. 24, pp. 227–234, 1995.
- [10] S. S. Chen, D. L. Donoho, and M. A. Saunders, "Atomic decomposition by basis pursuit," *SIAM J. Sci. Comput.*, vol. 20, no. 1, pp. 33–61, 1998.
- [11] E. J. Candès, J. K. Romberg, and T. Tao, "Stable signal recovery from incomplete and inaccurate measurements," *Comm. Pure Appl. Math.*, vol. 59, no. 8, pp. 1207–1223, Aug. 2006.
- [12] E. Candès and T. Tao, "The Dantzig selector: Statistical estimation when  $p$  is much larger than  $n$ ," *Ann. Stat.*, vol. 35, no. 6, pp. 2313–2351, Dec. 2007.
- [13] M. A. T. Figueiredo, R. D. Nowak, and S. J. Wright, "Gradient projection for sparse reconstruction: Application to compressed sensing and other inverse problems," *IEEE J. Sel. Topics Signal Process.*, vol. 1, no. 4, pp. 586–597, 2007.
- [14] Z. Wen, W. Yin, D. Goldfarb, and Y. Zhang, "A fast algorithm for sparse reconstruction based on shrinkage, subspace optimization, and continuation," *SIAM J. Sci. Comput.*, vol. 32, no. 4, pp. 1832–1857, 2010.
- [15] D. Donoho, A. Maleki, and A. Montanari, "Message-passing algorithms for compressed sensing," *Proc. Nat. Acad. Sci.*, vol. 106, no. 45, pp. 18914–18919, 2009.
- [16] S. Mallat and Z. Zhang, "Matching pursuits with time-frequency dictionaries," *IEEE Trans. Signal Process.*, vol. 41, no. 12, pp. 3397–3415, Dec. 1993.
- [17] J. Tropp, "Greed is good: Algorithmic results for sparse approximation," *IEEE Trans. Inf. Theory*, vol. 50, no. 10, pp. 2231–2242, Oct. 2004.
- [18] J. Tropp and A. Gilbert, "Signal recovery from random measurements via orthogonal matching pursuit," *IEEE Trans. Inf. Theory*, vol. 53, no. 12, pp. 4655–4666, Dec. 2007.
- [19] D. Needell and J. A. Tropp, "CoSaMP: Iterative signal recovery from incomplete and inaccurate samples," *Appl. Comput. Harmon. Anal.*, vol. 26, no. 3, pp. 301–321, May 2009.
- [20] L. Mancera and J. Portilla, " $\ell_0$ -norm-based sparse representation through alternate projections," in *Proc. IEEE Int. Conf. Image Process.*, Atlanta, GA, Oct. 2006, pp. 2089–2092.
- [21] K. Herrity, A. Gilbert, and J. Tropp, "Sparse approximation via iterative thresholding," in *Proc. IEEE Int. Conf. Acoust., Speech, Signal Process.*, Toulouse, France, May 2006, vol. 3, pp. 624–627.
- [22] T. Blumensath and M. E. Davies, "Iterative thresholding for sparse approximations," *J. Fourier Anal. Appl.*, vol. 14, no. 5–6, pp. 629–654, 2008.
- [23] T. Blumensath and M. E. Davies, "Iterative hard thresholding for compressed sensing," *Appl. Comput. Harmon. Anal.*, vol. 27, no. 3, pp. 265–274, 2009.
- [24] T. Blumensath and M. E. Davies, "Normalized iterative hard thresholding: Guaranteed stability and performance," *IEEE J. Sel. Topics Signal Process.*, vol. 4, pp. 298–309, Apr. 2010.
- [25] D. Wipf and B. Rao, "Sparse Bayesian learning for basis selection," *IEEE Trans. Signal Process.*, vol. 52, no. 8, pp. 2153–2164, 2004.
- [26] S. Ji, Y. Xue, and L. Carin, "Bayesian compressive sensing," *IEEE Trans. Signal Process.*, vol. 56, no. 6, pp. 2346–2356, 2008.
- [27] K. Qiu and A. Dogandžić, "Variance-component based sparse signal reconstruction and model selection," *IEEE Trans. Signal Process.*, vol. 58, pp. 2935–2952, Jun. 2010.

- [28] A. Dogandžić and K. Qiu, D. O. Thompson and D. E. Chimenti, Eds., "Automatic hard thresholding for sparse signal reconstruction from NDE measurements," in *Rev. Progr. Quantitative Nondestructive Evaluation, ser. AIP Conf. Proc.*, Melville, NY, 2010, vol. 29, pp. 806–813.
- [29] K. Qiu and A. Dogandžić, "Double overrelaxation thresholding methods for sparse signal reconstruction," in *Proc. 44th Annu. Conf. Inf. Sci. Syst.*, Princeton, NJ, Mar. 2010, pp. 1–6.
- [30] A. Maleki and D. L. Donoho, "Optimally tuned iterative thresholding algorithms for compressed sensing," *IEEE J. Sel. Topics Signal Process.*, vol. 4, pp. 330–341, Apr. 2010.
- [31] G. J. McLachlan and T. Krishnan, *The EM Algorithm and Extensions*, 2nd ed. New York: Wiley, 2008.
- [32] S. M. Kay, *Fundamentals of Statistical Signal Processing: Estimation Theory*. Englewood Cliffs, NJ: Prentice-Hall, 1993.
- [33] Y. He and C. Liu, "The dynamic 'expectation-conditional maximization either' algorithm," *J. Roy. Stat. Soc. Ser. B*, vol. 74, no. 2, pp. 313–336, 2012.
- [34] K. Qiu and A. Dogandžić, "ECME hard thresholding methods for image reconstruction from compressive samples," in *Applications of Digital Image Processing XXXIII*, ser. Proc. SPIE Optics & Photonics, A. G. Tescher, Ed. San Diego, CA: SPIE, 2010, vol. 7798.
- [35] T. Blumensath, "Accelerated iterative hard thresholding," *Signal Process.*, vol. 92, no. 3, pp. 752–756, 2012.
- [36] S. M. Kay, *Fundamentals of Statistical Signal Processing: Detection Theory*. Englewood Cliffs, NJ: Prentice-Hall, 1998.
- [37] R. A. Thisted, *Elements of Statistical Computing: Numerical Computation*. London, U.K.: Chapman & Hall, 1988.
- [38] C. Liu and D. B. Rubin, "The ECME algorithm: A simple extension of EM and ECM with faster monotone convergence," *Biometrika*, vol. 81, no. 4, pp. 633–648, 1994.
- [39] I. Daubechies, *Ten Lectures on Wavelets*. Philadelphia, PA: SIAM, 1992, vol. 61.
- [40] E. Candès and J. Romberg, C. A. Bouman and E. L. Miller, Eds., "Signal recovery from random projections," in *Proc. Computational Imaging III*, San Jose, CA, Jan. 2005, vol. 5674, pp. 76–86.
- [41] A. C. Kak and M. Slaney, *Principles of Computerized Tomographic Imaging*. New York: IEEE Press, 1988.
- [42] J. Fessler and B. Sutton, "Nonuniform fast Fourier transforms using min-max interpolation," *IEEE Trans. Signal Process.*, vol. 51, no. 2, pp. 560–574, Feb. 2003.
- [43] A. Dogandžić, R. Gu, and K. Qiu, "Mask iterative hard thresholding algorithms for sparse image reconstruction of objects with known contour," in *Proc. Asilomar Conf. Signals, Syst., Comput.*, Pacific Grove, CA, Nov. 2011, pp. 2111–2116.
- [44] D. A. Harville, *Matrix Algebra From a Statistician's Perspective*. New York: Springer-Verlag, 1997.
- [45] S. Colley, *Vector Calculus*, 3rd ed. Upper Saddle River, NJ: Prentice-Hall, 2006.



**Kun Qiu** was born in Shanghai, China. He received the B.S. degree in electrical engineering from Fudan University, Shanghai, China, in 2006, and Ph.D. degree in electrical engineering from Iowa State University, Ames, in 2011.

He is currently a staff scientist with the SAS Institute, Inc., San Diego, CA.



**Aleksandar Dogandžić** (S'96–M'01–SM'06) received the Dipl.Ing. degree (*summa cum laude*) in electrical engineering from the University of Belgrade, Yugoslavia, in 1995 and the M.S. and Ph.D. degrees in electrical engineering and computer science from the University of Illinois at Chicago (UIC) in 1997 and 2001, respectively.

In August 2001, he joined the Department of Electrical and Computer Engineering, Iowa State University (ISU), Ames, where he is currently an Associate Professor. His research interests are in statistical signal processing: theory and applications.

Dr. Dogandžić received the 2003 Young Author Best Paper Award and 2004 Signal Processing Magazine Best Paper Award, both by the IEEE Signal Processing Society. In 2006, he received the CAREER Award by the National Science Foundation. At ISU, he was awarded the 2006–2007 Litton Industries Assistant Professorship in Electrical and Computer Engineering. Dr. Dogandžić is currently an Associate Editor for the IEEE SIGNAL PROCESSING LETTERS and has previously served on the Editorial Board of the IEEE TRANSACTIONS ON SIGNAL PROCESSING. He served as a General Co-Chair of the Fourth International Workshop on Computational Advances in Multi-Sensor Adaptive Processing (CAMSAP) 2011.